Investigating the Antiviral Therapeutic Potentialities of Marine Polycyclic Lamellarin Pyrrole Alkaloids as Promising Inhibitors for SARS-CoV-2 and Zika Main Proteases (Mpro)

Florbela Pereira[1]*, Loay Bedda[2,3], Mohamed A. Tammam[4], Abdul Kader Alabdullah[5] Reem K. Arafa [2,3]* and Amr El-Demerdash[6,7]*

[1]LAQV-REQUIMTE, Department of Chemistry, NOVA School of Science and Technology, Universidade Nova de Lisboa, 2829-516 Caparica, Portugal

[2]Drug Design and Discovery Laboratory, Helmy Institute for Medical Sciences, Zewail City of Science and Technology, Giza 12578, Egypt

[3] Biomedical Sciences Program, University of Science and Technology, Zewail City of Science and Technology, Giza 12578, Egypt

[4]Department of Biochemistry, Faculty of Agriculture, Fayoum University, Fayoum 63514, Egypt

[5] Crop Genetics Department, John Innes Centre, Colney, Norwich NR4 7UH, UK

[6] Division of Organic Chemistry, Department of Chemistry, Faculty of Sciences, Mansoura University, Mansoura 35516, Egypt

[7] Department of Biochemistry and Metabolism, the John Innes Centre, Norwich Research Park, Norwich NR4 7UH, UK

---

*Correspondences:

Florbela Pereira florbela.pereira@fct.unl.pt

Reem K. Arafa rkhidr@zewailcity.edu.eg

Amr El-Demerdash a_eldemerdash83@mans.edu.eg, Amr.El-Demerdash@jic.ac.uk

Highlights

- SARS-Cov-2 (COVID-19) and Zika virus are two worldwide health crises
- Marine natural products (MNPs) are robust chemicals that might be able to compete these viral outbreaks.
- Integrated computational screening boosted with structure-activity relationships (SARs) studies are highly recommending the lamellarins marine pyrrole alkaloids (LPAs), in particular [lamellarin H (**14**)/lamellarin K (**17**)] and [lamellarin S (**26**)/ lamellarin Z (**39**)] as promising antiviral hits for hunting SARS-CoV-2 and Zika main proteases (Mpro) respectively, based on their excellent ligand-protein energy scores and relevant binding affinities with (Mpro) pocket residues.

Keywords: SARS-CoV-2; Zika virus; antiviral; virtual screening; molecular docking; molecular dynamics simulation; marine sponges, lamellarins, pyrrole alkaloids, structure-activity relationships.

Abbreviations:

ADME: Absorption, Distribution, Metabolism, and Excretion

COVID-19: Coronavirus Disease 2019

HIV: Human Immunodeficiency Virus

Rg: Radius of Gyration

LPAs: Lamellarins Pyrrole Alkaloids

MNPs: Marine Natural Products

Mpro: Main Protease

MDock: Molecular Docking

MD: Molecular Dynamic Simulations

MM-GBSA: Molecular Mechanics-Generalized Born Surface Area

PB: Poisson-Boltzmann

SARS-CoV-2: Severe Acute Respiratory Syndrome-Coronavirus 2

SARs: Structure-Activity Relationships

SASA: Solvent Accessible Surface Area

VMD: Visual Molecular Dynamics

RMSD: Root Mean Square Deviation

UFF: Universal Force Field

ZIKV: Zika Virus

Graphical abstract

A focused list of 39 lamellarin marine pyrrole alkaloids (**LAPs**) were comprehensively investigated for their antiviral therapeutic potentialities against SARS-CoV-2 and Zika main proteases (Mpro) using a set of integrated modern computational tools including molecular docking (MDocking), molecular dynamic simulations (MDS) and Structure activity relationships (SARs). Particularly, [lamellarin H (**14**)/lamellarin K (**17**)] and [lamellarin S (**26**)/ lamellarin Z (**39**)] were identified as promising antiviral hits for hunting SARS-CoV-2 and Zika main proteases (Mpro) respectively, based on their excellent ligand-protein energy scores and relevant binding affinities with (Mpro) pocket residues.

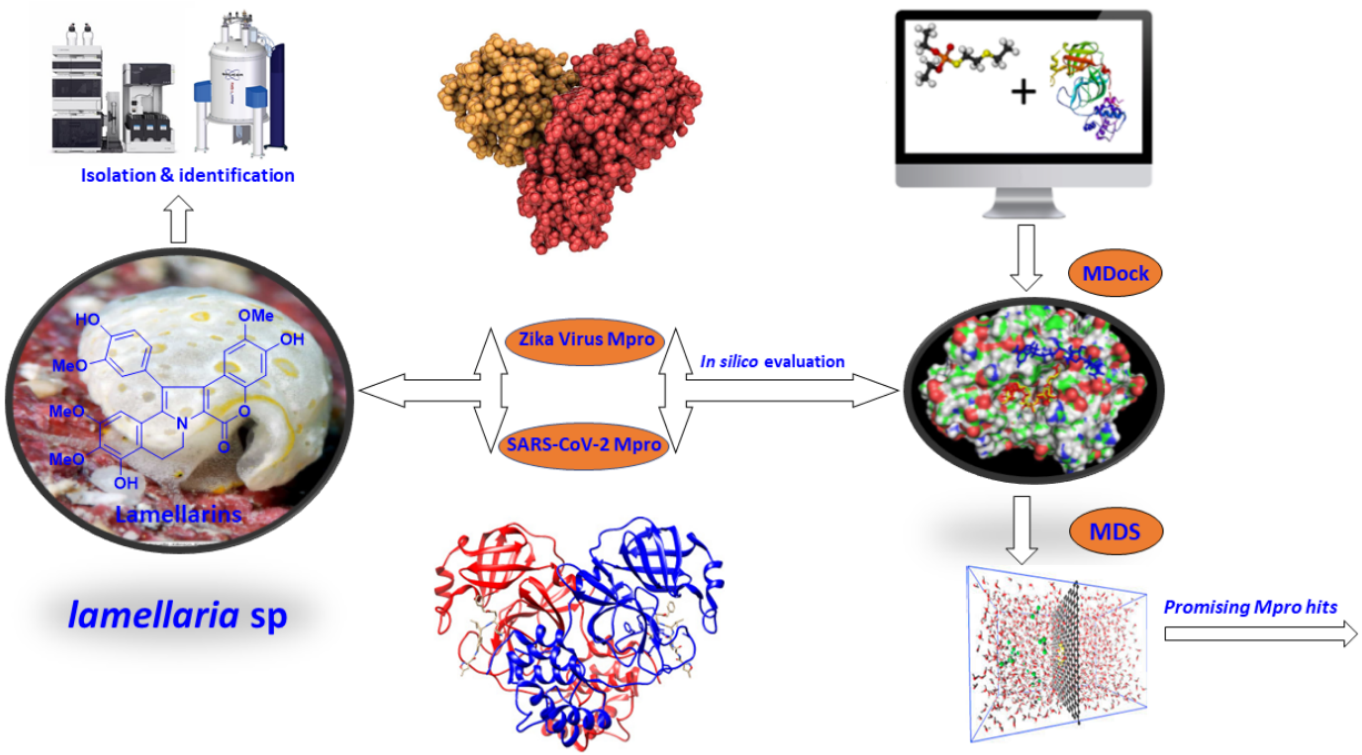

Abstract: The new coronavirus variant (SARS-CoV-2) and Zika virus are two worldwide health pandemics which outbreak borders and causing significant health difficulties, severe economic problems, and disturbing people's daily life globally. Although many forms of preventative vaccines have been discovered and approved as protective manipulations alongside several orally available medications to stop the viral explosion, parallel competent antivirals are vitally needed to compete these viruses and their forms. Along history, naturally occurring organic chemicals have always crucially recognized as a main source of valuable medications. Taking into consideration the SARS-CoV-2 and Zika main proteases (Mpro) as the re-production key element of the viral cycle and its main target, herein we report an intensive computer-aided virtual screening for a focused list of 39 marine lamellarins pyrrole alkaloids, against SARS-CoV-2 and Zika main proteases (Mpro) using a set of combined modern computational methodologies including molecular docking (MDock), molecule dynamic simulations (MDS) and structure-activity relationships (SARs) as well. Indeed, the molecular docking studies had revealed four promising marine alkaloids including [lamellarin H (**14**)/lamellarin K (**17**)] and [lamellarin S (**26**)/ lamellarin Z (**39**)], according to their notable ligand-protein energy scores and relevant binding affinities with the SARS-CoV-2 and Zika (Mpro) pocket residues, respectively. Consequentially, these four chemical hits were further examined thermodynamically though investigating their MD simulations at 100 ns, where they showed prominent stability within the accommodated (Mpro) pockets. Moreover, in-deep SARs studies suggested the crucial roles of the rigid fused polycyclic ring system, particularly aromatic A- and F- rings, position of the phenolic -OH and δ-lactone functionalities as essential structural and pharmacophoric characteristics for an effective protein ligand interaction against SARS-CoV-2 and Zika Mpro, respectively. These motivating outcomes are greatly recommending further *in vitro/vivo* examinations regarding those marine derived compounds and their synthetic congeners, opening the gate to identify clinically useful antivirals based or bio-inspired from lamellarins pyrrole alkaloids (**LPAs**).

1. Introduction

Viruses are subcellular infectious biological agents that rely on the host cell to replicate and complete their life cycle. On their own, viruses lack the complete machinery and energy necessary for their propagation. Viral propagation requires the transcription of viral mRNA, translation of viral proteins, and viral genome replication [1]. The dependence on the host cell to accomplish these processes varies among viruses and largely relates to the nature (DNA or RNA) and the complexity of their genomes. Viruses generally rely less on host functions when their genomes encode one or more of the enzymes required for sustaining virus replication in the cell, such as the viral polymerases [2] and viral proteases [3].

Although having extremely small genomes compared with the human genome, viruses adopted several unconventional transcriptional and translational strategies to greatly expand the coding potential of their small genomes [4]. This involves the use of overlapping genes [5], decoding subgenomic RNAs [6], programmed ribosomal frameshifting [7], leaky scanning, translation reinitiation, and ribosomal shunting [8].

Another strategy to increase the number of coded proteins from the compacted virus genome is the use of protease activity. Many viruses encode one or more proteases, where the viral genome encodes a polyprotein with an embedded viral protease that cleaves the polyprotein at several sites to produce mature proteins required to produce new infectious virions. Viral proteases are, therefore, vital for virus replication and infectivity [3]. Proteases have been identified in a wide range of viruses, including those responsible for notable human diseases like human immunodeficiency virus [9], hepatitis C virus [10], rubella virus [11], polio virus [12], foot-and-mouth disease virus [13], Dengue virus [14], Zika virus [15], and most recently Severe Acute Respiratory Syndrome Coronavirus-2 [16].

Proteases, like other enzymes, possess an active site that consists of a binding site and a catalytic site. For catalytic action to happen, the active site should bind to a certain amino acid sequence, called the cleavage site, in the targeted protein (substrate) [17]. The proteolytic cleavage sites recognized by a viral protease are largely diverse and processed at different rates according to the sequential order of the polyprotein processing [3]. Compared to cellular proteases, viral proteases are generally smaller in size and show low sequence similarity, even when sharing the same folding structure. Because of that, most

viral proteases have unique substrate specificity, which has considerable implications for the design and development of potent antiviral molecules [3]. The latest advances in structural biology methods like x-ray crystallography [18] and NMR spectroscopy [19] contributed significantly to increasing our knowledge of the viral proteases' structure and dynamics, which made them an attractive target for the development of novel antiviral drugs.

Severe Acute Respiratory Syndrome Coronavirus-2 (SARS-CoV-2) is a novel human coronavirus that is responsible for the pandemic disease COVID-19. Since the beginning of the COVID-19 outbreak, in December 2019, SARS-CoV-2 has infected more than 230 million people and caused 4.87 million deaths [20]. SARS-CoV-2 belongs to the lineage B of genus β-coronavirus that also includes Middle East respiratory syndrome (MERS) and severe acute respiratory syndrome coronavirus (SARS-CoV-2). SARS-CoV-2 was named after SARS-CoV-2 because of their high genome sequence identity (79.6%), although, the highest sequence identity with other coronaviruses reached 96% with bat coronavirus RaTG13 [21, 22].

Vaccination programs are the main measure currently used worldwide for the prevention of SARS-CoV-2 infection. Although, some effective vaccines and drugs have already been authorized for emergency use [23-25], the emergence of new variants of the virus makes it urgent to identify alternative targets and develop more broad-spectrum antiviral agents for treating COVID-19 [26].

Structurally, the SARS-CoV-2 coronavirus is an enveloped virus with a helical nucleocapsid that contains one of the largest positive single-stranded RNA genomes (ca. 30 kb). The virions have ellipsoidal and spherical shape with average diameter ranges between 65 nm to 97 nm [27]. The viral envelope is comprised of a bilayer lipid membrane that is speckled with glycoprotein spikes (S), that give the virus its crown-like appearance [28], membrane (M) protein, and envelop (E) glycoprotein. (**Figure 1A**). The virion contains another structural protein, known as nucleocapsid (N) phosphoprotein, which is a basic RNA-binding protein that complexes and protects the genome [29].

The SARS-CoV-2 genome contains fourteen open reading frames (ORFs) that encode 28 proteins through different transcriptional, translational, and post-translational strategies (**Figure 1B**). The first two ORFs (ORF1a and ORF1b) occupy the 5′-two-thirds of the viral genome and directly translated into two polyproteins (pp1a and pp1ab) due to a

ribosomal frameshifting mechanism. The two polyproteins are, then, cleaved by two viral proteases, papain-like protease (PLpro) and 3C-like or main-protease (Mpro) into sixteen non-structural proteins (Nsp1–Nsp16) essential for the viral replication translation complex [30, 31]. The rest of the ORFs are translated indirectly from the viral genome through sub-genomic RNAs to produce the four structural proteins (S, M, E, and N) and several accessory proteins (3a, 3b, 6, 7a, 7b, 8, 9b, 9c, and 10) (**Figure 1C**) [32].

The Mpro, is a cysteine protease with an atomic mass of 33.8 kDa that is responsible of processing the viral polyproteins pp1a and pp1ab at 11 cleavage sites at least. Therefore, it is responsible for the formation of most of the functional non-structural proteins. The lack of homologous human proteins, together with the crucial role of Mpro in virus propagation make it an ideal target for the development of anti-SARS-CoV-2 drugs [16].

Concerning Zika virus (ZIKV), is a human pathogen responsible for a devastating epidemic in the Americas and still jeopardizes public health. ZIKV is a mosquito-borne virus belongs to the family Flaviviridae that contains several viruses of clinical importance such as dengue virus (DENV) and West Nile virus (WNV) [33-35]. ZIKV was first isolated in 1947 from a macaque monkey in the Zika Forest in Uganda [36]. Then, in 1954, the first human infection was reported in Nigeria, however, it remains limited to sporadic cases in Africa and Asia causing mild disease in about 20% of infected people. The first outbreak of Zika virus occurred in 2007 in Yap. But it became a serious public health concern in 2015 when a large outbreak occurred in Brazil and rapidly spread in the Americas resulting in more than 700,000 cases with occasional miscarriage and severe congenital birth defects, such as fatal microcephaly, intrauterine growth restriction, and other neurodevelopmental malformations [37, 38].

The ZIKV virion comprises of a spherical envelope (approximately 50 nm in diameter) and an icosahedral nucleocapsid (approximately 30 nm in diameter) surrounding the viral RNA genome (**Figure 2A**). The enveloped consists of 90 heterodimers of the membrane (M) protein and the envelope (E) glycoprotein embedded in a lipid bilayer membrane. The nucleocapsid is made of multiple copies of the capsid (C) protein [39]. The viral genome is a positive single-stranded RNA with a size of *ca.* 10.8 kilobases. It contains a single open reading frame (ORF) flanked by the 5’ and 3’ untranslated regions (UTRs) (**Figure 2B**). The ORF encodes a polyprotein precursor (3423 amino acids in length) that is post-translationally cleaved by the viral and cellular proteases into three structural proteins to produce the three structural proteins (C, PrM, and E) and seven non-structural

proteins (NS1, NS2A, NS2B, NS3, NS4A, NS4B, and NS5) (**Figure 2C**) [40]. The structural proteins are essential components of the virion and are involved in viral entry, fusion, and assembly, while the non-structural proteins are mainly involved in viral RNA replication, viral protein processing, and regulation of the host cell responses. NS1 is involved in viral replication, infection, and interacts with the host immune factors when secreted extracellularly for immune evasion and pathogenesis [41]. NS3 consists of a protease domain that linked to NS2B to form a protease complex [15, 40, 42]. NS5 contains RNA-dependent RNA polymerase (RdRp) and methyltransferase (MTase) domains essential for viral replication, translation, and evasion of host immune response [43]. The Zika virus protease is a serine protease with a catalytic triad formed by three residues, His51, Asp75, and Ser135, in its active site in the N-terminal region of NS3 and required a small hydrophilic proportion of NS2B as cofactor domain [44]. The protease of ZIKV is responsible for cleaving four joints between non-structural proteins (NS2A/NS2B, NS2B/NS3, NS3/NS4A, and NS4B/NS5) and two sites within the C protein (C/Ci) and NS4A (NS4A/2K), which are essential to release functionally structural and non-structural proteins [15, 44, 45]. Hence, inhibiting the protease activity of the Zika virus represents an important strategy in the fight against this virus.

Figure 1. SARS-CoV-2

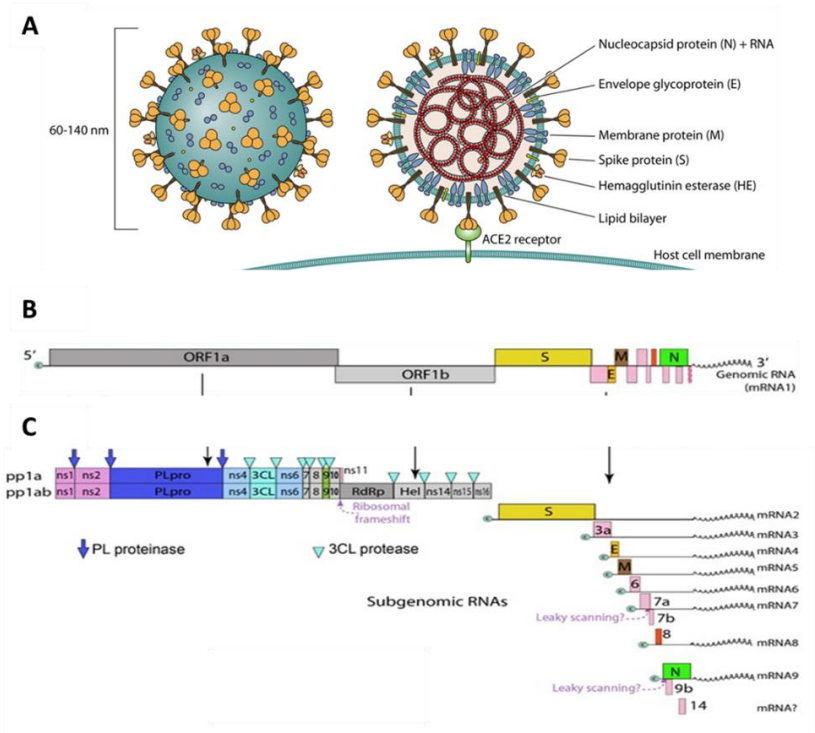

Figure 1: Structural composition of SARS-CoV-2

Figure 2. Zika virus

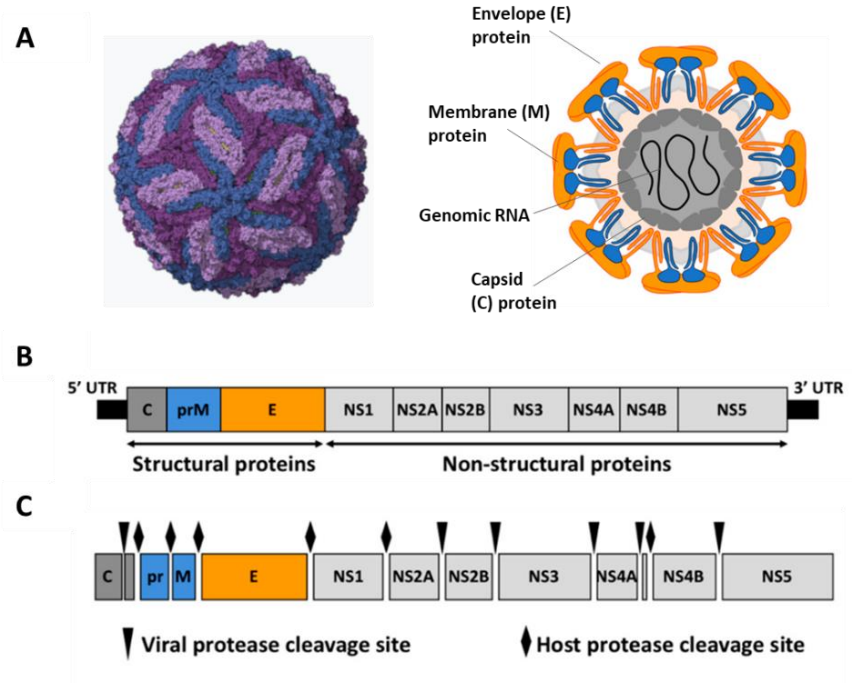

Figure 2: Structural composition of Zika virus

Over span of human history, naturally occurring organic chemicals were extensively used as primary treatments of a variety of medical challenges. Indeed, natural products have played central roles within drug discovery programs. Intriguingly, they display unique, diverse, and complex structural features compared to synthetic medicine, that enhance the drug discovery processes [46-49]. Since 1950's, marine natural products (**MNPs**) and their synthetic analogues have been emerged as a revolutionary chemical space which possess unprecedented diversification of molecular articturings with novel therapeutic actions [50-52]. Up to date, 17 marine derived natural products have been clinically approved as effective medications for numerous challenging diseases, whilst further 20 marine molecules are currently being investigated and developed within different clinical and preclinical phases [53-55].

Lamellarins are fascinating class of a broad family of marine polycyclic pyrrole derived alkaloids reported from numerous marine organisms including molluscs, ascidians, tunicates, and sponges. In 1985, Faulkner *et al*., reported the discovered the first four members lamellarins A-D from the prosobranch mollusk, *Lamellaria* sp., collected near Koror, Palau [56-59]. Up to date, over 70 lamellarins and structurally related congeners have been reported, including other classes namely ningalins, lukianols, polycitones, and storniamides [60-62]. Chemically, they are featuring of a common a polyaromatic ring

system incooperating a central fused pyrrole scaffold, where positions 3 and 4 are decorated by polyhydroxy- or methoxyphenyl groups (aromatic A-, E-, and F-rings), and the 5,6-bond on ring D can be either saturated or unsaturated [60].

Structurally, they are classified into three main categories; **type I** involving the majority of reported lamellarins and process a fused fully substituted central pyrrolic moiety of 14-phenyl-6H-[1]benzopyrano[4' ,3' :4,5] pyrrolo[2,1-a]isoquinoline ring system. **Type II** bears a simpler non fused trisubstituted pyrrole of 3,4-diarylpyrrole-2-carboxylate ring system. **Type III** are some water-soluble sulphated derivatives of **type I** fused lamellarins. Biomimetically, lamellarins pyrrolic alkaloids could be biosynthetically derived from a sequential enzymatic transformation of aromatic amino acids like tyrosine and 3,4-dihydroxyphenylalanine (**Figure 3**) [60].

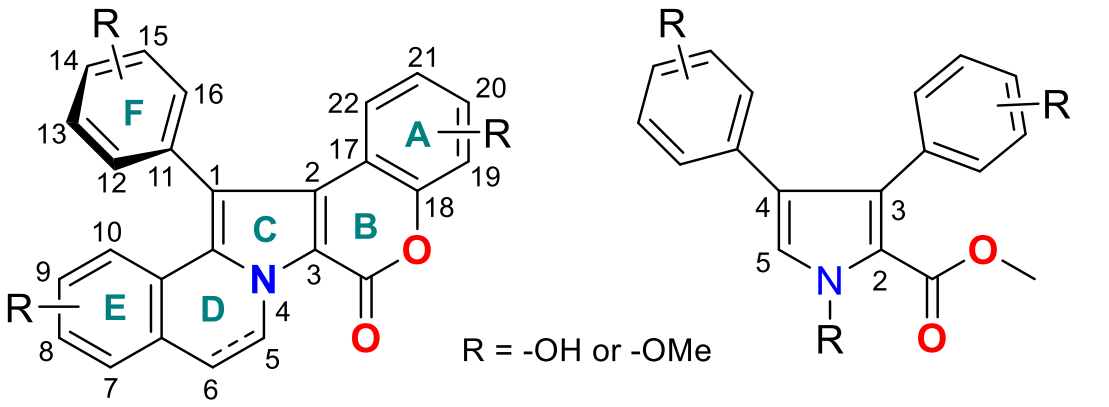

Type I: Fused lamellarines **Type II**: non-fused lamellarines

Figure 3: Representative common scaffolds of fused/non-fused lamellarins.

Pharmacologically, lamellarins pyrrole alkaloids (**LPAs**) displayed a myriad of intriguing powerful biomedical potentialities including, cytotoxicity and topoisomerase I-mediated DNA cleavage antitumor activities [63-66], mitochondrial function inhibitors [67-69], protein kinases inhibitors [70-72], multidrug resistance reversal activity [73-75]. Interestingly, a notable n umber of LPAs disclosed vigorous antiviral activity in particular as Anti-HIV-1. Indeed, the lamellarin A 20-sulphated compound showed potent terminal cleavage inhibitory activity with an IC_{50} = 16 μM and strand transfer activity with an IC_{50} = 22 μM against a purified integrase enzyme. Moreover, it disclosed significant inhibitory activity against the early steps of HIV-1 replication at low to sub-micromolar ranges [76].

Moreover, the non-sulphated congeners of lamellarin A (**1**) displayed no inhibitory activity against the HIV-1 integrase enzyme at concentration 1.6 mM compared to the mono- and di-sulphated analogues [lamellarin A 20-sulfate and 13,20-disulfate], they showed robust integrase enzyme inhibitory activity with IC_{50} values 22 and 49 mM respectively. This might implies the central role of the sulphate group as a pharmacophoric key for the antiviral activity [77]. Furthermore, Kamiyama *et al*., comprehensively established formal total syntheses, structure-activity relationships (SARs) for numerous natural and synthetic fused and non-fused ring opened lamellarin A 20-sulphate analogues alongside their mechanism of action as anti-HIV-1 inhibitors. Extensively, all the tested pentacyclic lamellarin sulfated compounds showed significant anti-HIV-1 activity at concentration of 10 μM with disregarding the number/position of the sulphate functionality.

On contrary, non-sulphated and ring-opened lamellarin sulphate congeners showed no effect against the HIV-1 vector infection at identical concentrations. This might highlight the importance of both the lamellarin pentacyclic articturing core and the sulphate moiety as crucial pharmacophoric structural features for anti-HIV-1 activity and comes in constancy with former studies [77, 78].

Recently, in 2019, Eurtivong *et al*., investigated virtually through a molecule docking approach the antiviral profiling of 8 lamellarins type I compounds as promising HIV-1 integrase strand transfer complex. The authors highlighted that such oxygenated polyaromatic pyrrolic compounds are interacting effectively via hydrogen bonding with a key residue Glu92 beside other potential residues including Cys65, His67, Asp64 and Asp116 [79].

As a result of their powerful biomedical potentialities, and considering their limited natural quantities, lamellarins have attracted immensely worldwide organic chemists and pharmacists to scale up their availability though economic, effective, and practical synthetic strategies. Three elegant synesthetic tactics including pyrrole ring functionalization, cycloaddition/condensation reactions incooperating isoquinoline scaffold and coumarin derivatives approach were able to not only totally synthesising natural lamellarins, but also, getting structurally diversified congeners, which finally embark scientist to shape an integrated and systematic SARs mapping and provide more chemical entities for clinical trials. For recent and detailed advances on their chemical syntheses, see Fukuda *et al*., [60].

Taking in account the crucial role of SARS-CoV-2 (COVID-19 pandemic) and Zika main protases (Mpro) as infecting keys, alongside with the potent antiviral activities of the (**MNPs)** under examination, and as a part of our continuous program for identifying physiologically active marine natural products [80-85] with potential antiviral leads [86-89], herein we report a comprehensive virtual screening of 39 lamellarins pyrrole derive marine alkaloids (**LPAs**) against SARS-CoV-2 and Zika main proteases (Mpro) using an integrated set of advanced computational and bioinformatics tools including (MDock), (MD) simulations and (SARs).

2. Material and methods

2.1. Preparation of the Screening Library

A ChemDraw software (version 20) was used to draw the compounds and saved as MOL files. The optimization of the 3D structure of the 39 lamellarin-derived pyrrole marine alkaloids was performed with the Gaussian 09 program [90] using the hybrid method B3LYP and the base set 6-31G (d,p). [91, 92] The software program OpenBabel (version 2.3.1) [93] was used to convert the MOL2 files to PDBQT files.

2.2 Molecular Docking Studies (MDock)

PDBQT files were used for docking to SARS-CoV-2 Mpro enzyme (PDB ID: 6LU7) and Zika Mpro enzyme (PDB ID: 5H4I) with AutoDock Vina (version 1.1) [94]. Water molecules, ions and ligands were removed from SARS-CoV-2 (Mpro) enzyme (PDB ID: 6LU7) and Zika (Mpro) enzyme (PDB ID: 5H4I) prior to docking using the AutoDockTools (http://mgltools.scripps.edu/, accessed on 07 June 2022). The coordinates of the search space for SARS-CoV-2 (Mpro) and Zika (Mpro) enzymes were maximized to allow the entire macromolecule to be considered for docking. The search space coordinates were SARS-CoV-2 (Mpro) enzyme; Centre X: -12.207 Y: 9.178 Z: 70.295, and Zika (Mpro) enzyme X: -6.077 Y: 3.496 Z: -17.334, Dimensions X: 40.000 Y: 40.000 Z: 40.000. Ligand tethering of the SARS-CoV-2 (Mpro) and Zika (Mpro) enzymes was performed by regulating the genetic algorithm (GA) parameters, using 10 runs of the GA criteria. The docking binding poses were visualized with PyMOL Molecular Graphics System, Version 2.0 Schrödinger, LLC, UCSF Chimera [95], and LigPlot^{+} v.2.2.5 [96].

2.3 Molecular Dynamics Simulations (MDS)

2.3.1 Molecular Dynamics Simulations Setup

The top two candidates obtained from molecular docking for each of Zika virus protease and SARS-CoV-2 main proteases (Mpro) were subjected to 100 ns simulations. Regarding the software packages, GROMACS 2020.3 was used to run the simulations and perform primary stability and binding analyses [97]. Protein topology files were created with the charmm36-jul2021 forcefield, whereas the ligands topology files were created with the official CHARMM General Force Field server (CGenFF). A dodecahedron box was created to contain the system with water molecules represented by the CHARMM-modified TIP3P water model (TIP3P_CHARMM). Furthermore, explicit solvent and periodic boundary conditions were applied, and the system was neutralized by the addition of sodium and chloride ions. Then, The steepest decent method was utilized to perform an energy minimization step of 5,000 steps to optimize the structure's geometry and prevent clashes. Subsequently, an NVT equilibration step was performed for 50,000 steps with position restraints on the ligands and the proteins to optimize the system at 310 °K temperature. Following that, an NPT equilibration step was performed with the same restraints to optimize the system at 1 bar pressure. Finally, the position restraints were released, and the simulation was run for 100 ns with a time step of 2 femtoseconds. The leap-frog integrator was used for the equilibration steps and the simulation run, while for the temperature coupling in the NVT step and the pressure coupling in the NPT step, the modified Berendsen thermostat and Parrinello-Rahman methods were used, respectively.

2.3.2 Free Energy Calculation Parameters

To assess the four compounds' binding affinity, we calculated free energy for each system. GMX_MMPBSA (v1.5.2) tool was used in conjunction with GROMACS to perform such calculations. GMX_MMPBSA is based on AMBER's robust MMPBSA.py tool [98, 99]. The first 50 ns were assumed to be an equilibration phase and were excluded from the analyses. Therefore, the free energy calculations were carried out for the last 50 ns of the simulations divided into 5000 frames. GMX_MMPBSA removed the PBC prior to the calculations. The analyses were performed on an interval of 2 frames, ending with a total of 2501 frames included in the calculations for each system. The free energy calculations were carried out using the Poisson-Boltzmann (PB) approach. AMBER's

topologies were generated using the new ff19SB for the proteins and the gaff forcefield for the ligands. Sodium and Chloride ions were represented by the frcmod.ions1lm_126_tip3p (Li/Merz ion parameters for +1 and -1 ions in TIP3P water).

Moreover, For building amber topologies, the recommended charm_radii were used to represent the PBRadii (PBRadii=7). No Entropic estimation was performed. As a result, the calculated binding energy value is not the exact real free energy value because entropy is not considered, but it is still a good representation of the relative binding energies. In the dielectric interface implementation, A level-set-based algebraic method is used. A single term proportional to the solvent's accessible surface area (SASA) is used to model the total non-polar solvation-free energy. Decomposition analysis was performed on residues within 6 angstroms of the ligand.

2.3.3 Molecular Dynamics Simulations Analysis

The top two molecular docking performers, lamellarin H (**14**) and lamellarin K (**17**), were subjected to 100 ns simulations while complexed with SARS-CoV-2 main protease (Mpro) for advanced stability and binding affinity analyses. Additionally, The top two compounds docked against Zika virus main protease (Mpro), lamellarin S (**26**) and lamellarin Z (**39**), have been also complexed and simulated for 100 ns.

2.4 *In-silico* Prediction of Physicochemical properties, Pharmacokinetic and Toxicity profiles

The pharmacokinetic properties of the most promising lamellarin-derived pyrrole alkaloids (**14, 17, 26 and 39**) were calculated using the SWISS-ADME platform (https://www.swissadme.ch, accessed on 04 September 2022) [100].

2.5. Identification of Marine Polycyclic Lamellarin Pyrrole Alkaloids (LPAs)

A focused library of 39 lamellarin-derived pyrrole alkaloids (**LPAs**) which processes fused **type I** skeleton (**Schemes 1-2**) were previously reported from several marine organism including molluscs, ascidians, tunicates, and sponges. For comprehensive detailed isolation, analytical and structural characterization studies, please see Fukuda *et al.*, [60, 61].

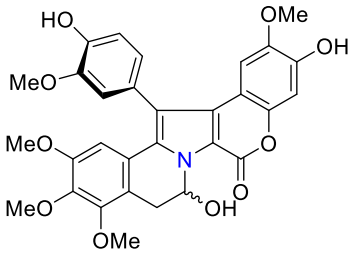

lamellarin A (**1**)

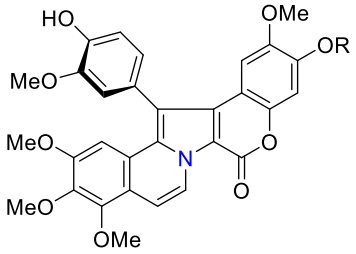

lamellarin B (**2**), R = H
lamellarin B 20 sulfate (**3**), R = SO_3Na

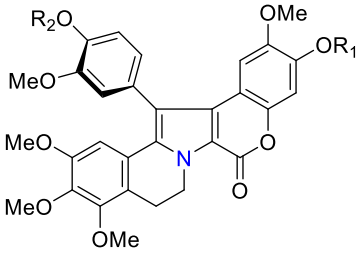

lamellarin C (**4**), R_1=R_2 = H
lamellarin C diacetate (**5**), R_1=R_2 = Ac
lamellarin C 20-sulfate (**6**), R_1=SO_3Na, R_2 = H

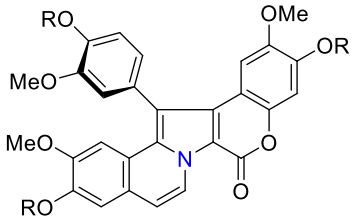

lamellarin D (**7**), R = H
lamellarin D triacetate (**8**), R = Ac

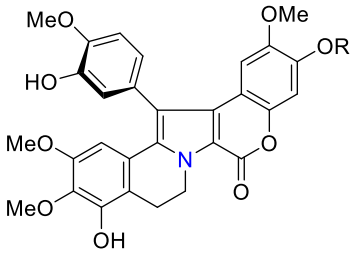

lamellarin E (**9**), R = H
lamellarin E 20-sulfate (**10**), R = SO_3Na

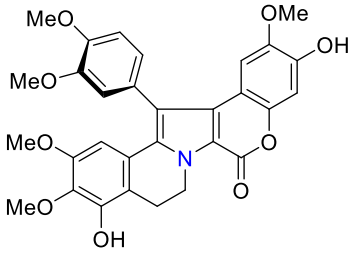

lamellarin F (**11**), R = H

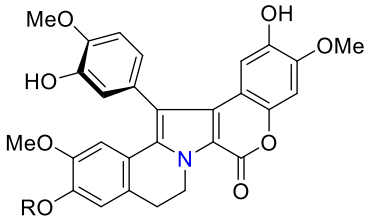

lamellarin G (**12**), R = H
lamellarin G 8-sulfate (**13**), R = SO_3Na

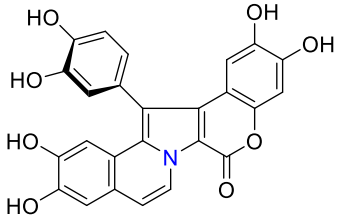

lamellarin H (**14**)

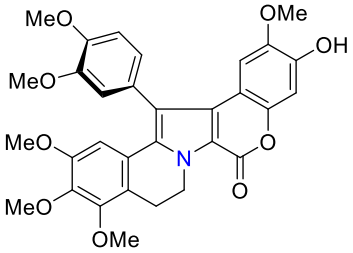

lamellarin **I** (**15**)

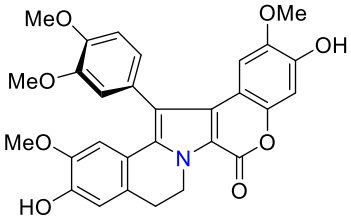

lamellarin J (**16**)

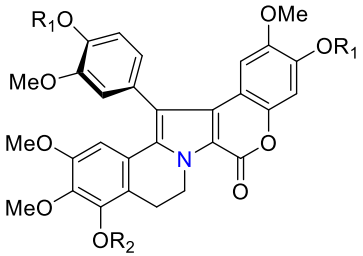

lamellarin K (**17**), R_1=R_2 = H
lamellarin K diacetate (**18**), R_1=Ac, R_2 = H
lamellarin K triacetate (**19**), R_1= R_2 = Ac

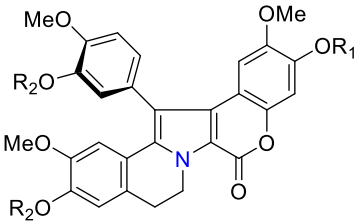

lamellarin L (**20**), R_1=R_2 = H
lamellarin L triacetate (**21**), R_1= R_2= Ac
lamellarin L 20-sulfate (**22**), R_1= SO_3Na, R_2 = H

Scheme 1. Reported lamellarin pyrrole alkaloids (**1-22**)

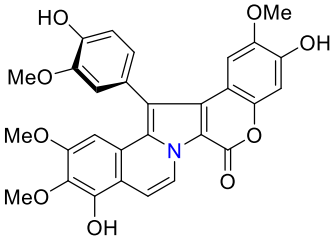

lamellarin M (**23**)

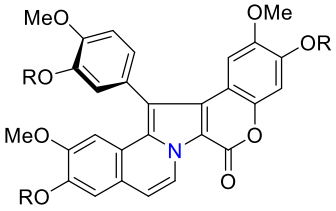

lamellarin N (**24**), R = H
lamellarin N triacetate (**25**), R =Ac

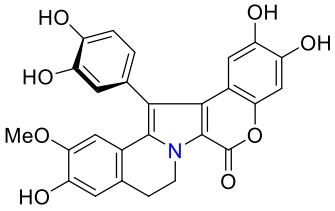

lamellarin S (**26**)

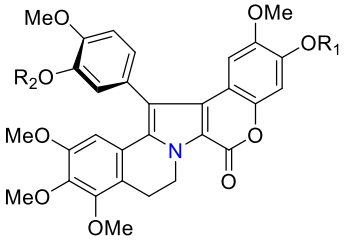

lamellarin T (**27**), R_1=R_2 = H
lamellarin T diacetate (**28**), R_1=R_2 =Ac
lamellarin T 20-sulfate (**29**), R_1= SO_3Na, R_2 =H

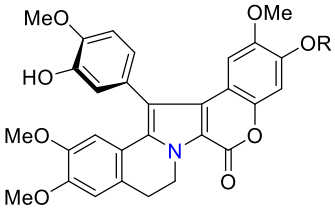

lamellarin U (**30**), R = H
lamellarin U 20-sulfate (**31**), R = SO_3Na

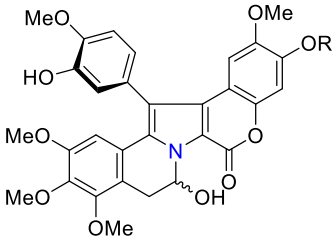

lamellarin V (**32**), R = H
lamellarin V 20-sulfate (**33**), R = SO_3Na

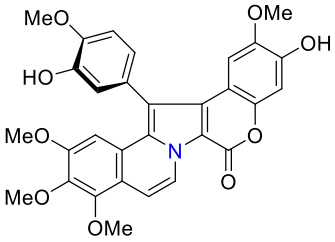

lamellarin W (**34**)

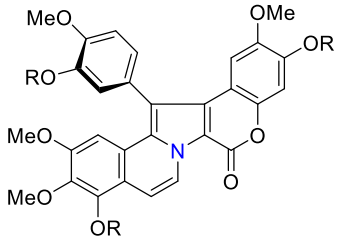

lamellarin X (**35**), R = H
lamellarin X triacetate (**36**), R = Ac

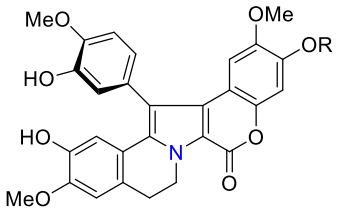

lamellarin Y (**37**), R = H
lamellarin Y 20-sulfate (**38**), R = SO_3Na

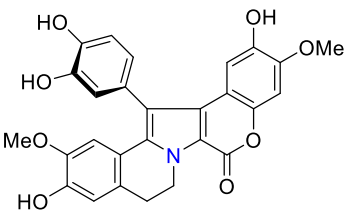

lamellarin Z (**39**)

Scheme 2. Reported lamellarin pyrrole alkaloids (**23-39**)

3. Results and Discussions

3.1. Molecular Docking (MDock) and Binding Energies Studies

Molecular docking (MDock) was applied to elucidate the binding action of 39 lamellarin pyrrole marine alkaloids against SARS-CoV-2 and Zika Mpro enzymes. Structural mechanistic analyses revealed four main sub-classes, including 15 hydroxyl and methoxy substituted lamellarin derivatives [A (**1**), C (**4**), E (**9**), F (**11**), G (**12**), I (**15**), J (**16**), K (**17**), L (**20**), S (**26**), T (**27**), U (**30**), V (**32**), T (**37**) and Z (**39**)], 8 acetate lamellarin derivatives: [C diacetate (**5**), D triacetate (**8**), K diacetate (**18**), K triacetate (**19**), L triacetate (**21**), N triacetate (**25**), T diacetate (**28**), X triacetate (**36**)], 9 sulfated lamellarin derivatives: [B 20-sulfate (**3**), C 20-sulfate (**6**), E 20-sulfate (**10**), G 8-sulfate (**13**), L 20-sulfate (**22**), T 20-sulfate (**29**), U 20-sulfate (**31**), V 20-sulfate (**33**), Y 20-sulfate (**38**) , and 7 hydroxyl and methoxy substituted with unsaturation in ring B lamellarin derivatives: [B (**2**), D (**7**), H (**14**), M (**23**), N (**24**), W (**34**), X (**35**)], (**Scheme 1-2**). In Table S1 of the *Supplementary Data*, the results of molecular docking using the AutoDock Vina software against the two viral targets, SARS-CoV-2 (Mpro) and Zika (Mpro) were represented and summarized. As shown in **Figure 4**, the best-docked poses for the positive control (**O6K**), were showed on SARS-CoV-2 Mpro (**A**) and Zika Mpro (**B**) enzymes.

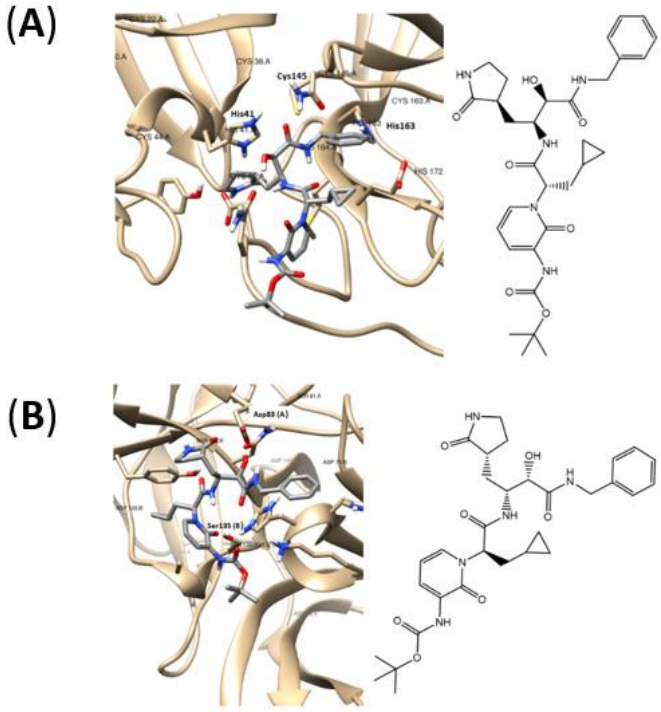

Figure 4. Interaction profiles of the best-docked poses for the positive control, O6K against: (**A**) SARS-CoV-2 M^{pro} and (**B**) Zika Mpro enzymes.

Indeed, a flexible molecular docking was used to perform the virtual screening of the 39 lamellarin derivatives to find the most favourable binding interactions, and the calculated free binding energies by the set of search space coordinates, which are reported in **Table 1** for the top 10 lamellarin derivatives selected for each target along with the positive control (**O6K**).

Table 1. Calculated free binding energies (ΔG_B, in kcal/mol) for the top 10 selected lamellarin derivatives and the positive control (**O6K)**, for each target, as well as their reported biological activities.

Lamellarins	**ΔG_B, in kcal/mol[a]**		**Reported Biological Activities**
	SARS-CoV-2 M^{pro}	**Zika M^{pro}**	
D (**7**)	---	-8.13	Potent inhibitor of Topoisomerase I [101]; cytotoxic activity against cancer cell lines e.g. HeLa, XC, Vero, MDCK (nM) [101].
E (**9**)	-8.40	---	---
G (**12**)	-8.57	-8.47	---
H (**14**)	**-9.37**	-8.40	Topoisomerase I (IC_{50} = 0.23 mM) [102].
J (**16**)	-8.47	-8.13	---
K (**17**)	**-9.40**	---	Toxic against Topoisomerase I [103].
L (**20**)	-8.67	-8.17	---
S (**26**)	-9.00	**-8.53**	---
U (**30**)	-8.47	-8.10	---
Z (**39**)	-9.30	**-8.63**	---
B 20-sulfate (**3**)	-8.40	---	---
G 8-sulfate (**13**)	---	-8.30	---
L 20-sulfate (**22**)	---	-8.30	---
(**O6K**)[b]	-7.90	-7.83	---

[a] The lamellarin derivatives selected have a calculated $\Delta G_B \leq$ -8.4 Kcal/mol and -8.1 Kcal/mol for SARS-CoV-2 Mpro and Zika Mpro, respectively. [b] Positive Control.

As can be seen in **Table 1** and **Figure 5**, there are 8 lamellarin derivatives marked in blue, namely [G (**12**), H (**14**), J (**16**), K (**17**), L (**20**), S (**26**), U (**30**) and Z (**39**)], which are simultaneously predicted to be the most promising SARS-CoV-2 Mpro and Zika Mpro inhibitors. Indeed, from those, seven lamellarin derivatives have hydroxyl functionalities at positions 7 (-A ring), 13 or 14 (-F ring) and either 20 or 21 (-E ring). These excellent binding affinities could be attributed to potential hydrogen bonds interactions between such highly hydroxylated positions and specific amino acid residues.

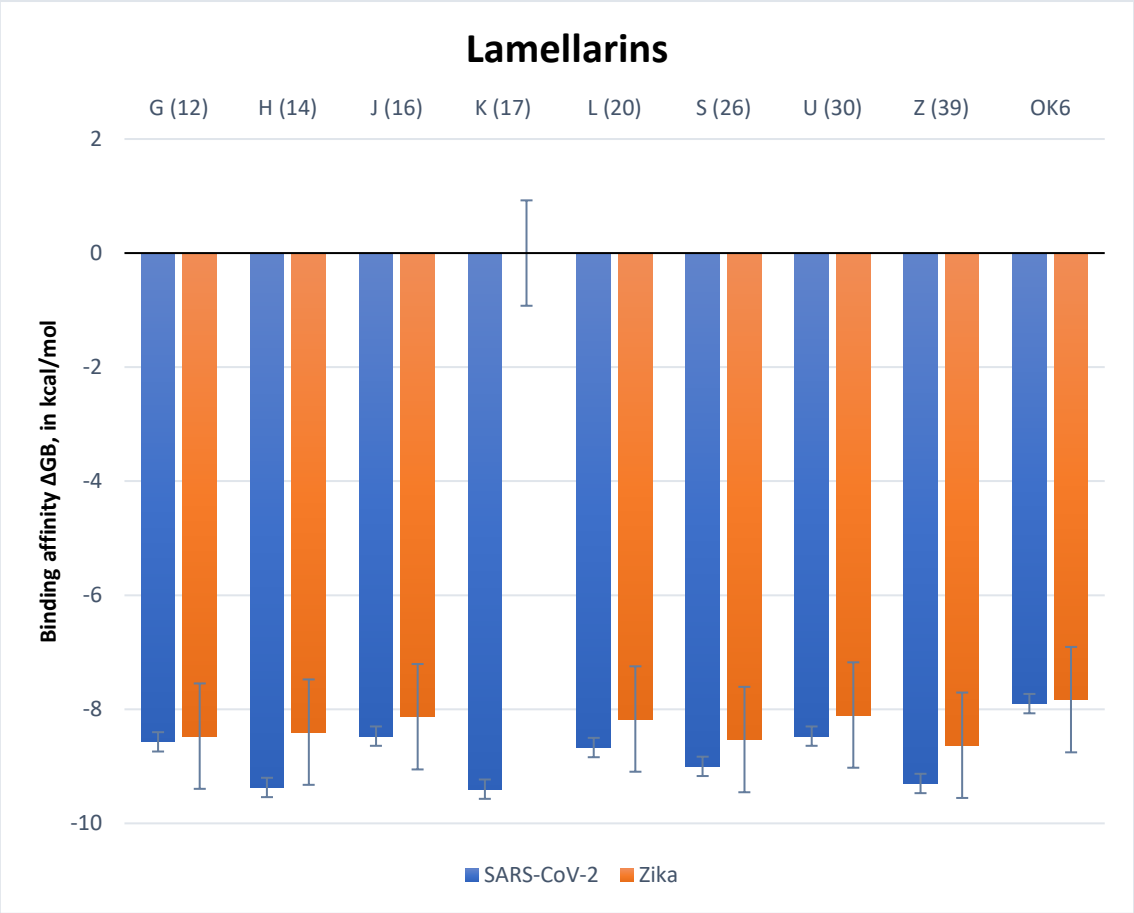

Figure 5: The calculated average binding energies of the 8 top tested lamellarin alkaloids against [SARS-CoV-2, (PDB ID: 6LU7)] and [Zika, (PDB ID: 5H4I)] Mpro along with the positive control (**O6K)**

3.1.1 SARS-CoV-2 Mpro

The derivatives with the lowest ΔG calculated, *i.e.*, the most promising derivatives, are lamellarin K (**17**), H (**14**), Z (**39**) and S (**26**) with values of -9.40, -9.37, -9.30, and -9.00 Kcal/mol, respectively (**Scheme 1-2**) and Table S1 of *the Supplementary Data*). Also, it worth mentions that the positive control (**O6k**), known antiviral agent, has a ΔG values calculated of -7.9 Kcal/mol. On the contrary, the lamellarin derivatives with the highest ΔG calculated, *i.e.*, the least promising derivatives, were lamellarin I (**15**), D triacetate (**8**) and K triacetate (**19**) with values of -7.67, -7.63, and -7.63 Kcal/mol, respectively (Scheme 1-2) and Table S1 of the *Supplementary Data).* In **Figure 6**, the interaction profiles of the best-docked poses for the lamellarin H (**14**) and lamellarin K (**17**) with SARS-CoV-2 Mpro were represented.

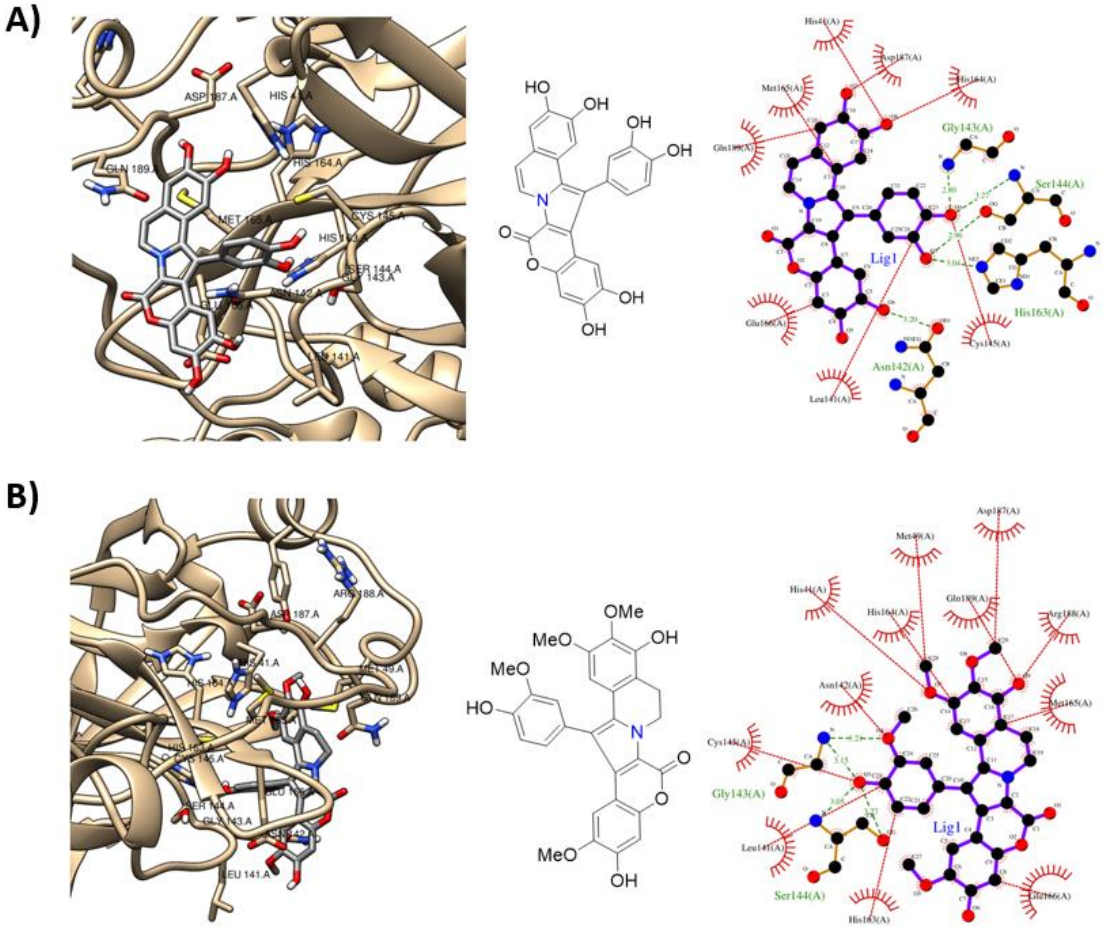

Figure 6. Interaction profiles of the best-docked poses: (**A**) for lamellarin H (**14**) and (**B**) for lamellarin K (**17**).

Intriguingly, the 14-OH functionality of lamellarin derivatives, found in ring -F apparently participates in potential hydrogen-bonding interactions with the side chains of Gly143 and Ser144 of the SARS-CoV-2 Mpro enzyme as can be seen in lamellarin H (**14**) and lamellarin K (**17**), **Figure 6**. Also very relevant are the hydrophobic interactions of the ring F with the Cys145 residue of the enzyme. Other relevant hydrophobic interaction is between the ring A and His41 residue of the enzyme. The double bond between C5 and C6 in ring B appear to be not essential for activity against SARS-CoV-2 Mpro, the lamellarin H (**14**) has the double bond however the lamellarin K (**17**) does not have.

3.1.2 Zika Mpro

The derivatives with the lowest ΔG calculated are lamellarin Z (**39**), S (**26**), G (**12**) and H (**14**) with values of -8.63, -8.53, -8.47, and -8.40 Kcal/mol, respectively (Scheme 1-2) and Table S1 of the *Supplementary Data*). As described before, it is also important to bear in mind that the positive control (O6k), known antiviral agent, has a ΔG value calculated of

-7.83 Kcal/mol. On the contrary, the lamellarin derivatives with the highest ΔG calculated were lamellarin T diacetate (**28**), Y 20-sulfate (**38**) and T 20-sulfate (**29**) with values of -6.87, -6.80, and -6.63 Kcal/mol, respectively (Scheme 1 and Table S1 of the *Supplementary Data*). As in **Figure 7**, the interaction profiles of the best-docked poses for the lamellarin S (**26**) and lamellarin Z (**39**) with Zika Mpro were represented.

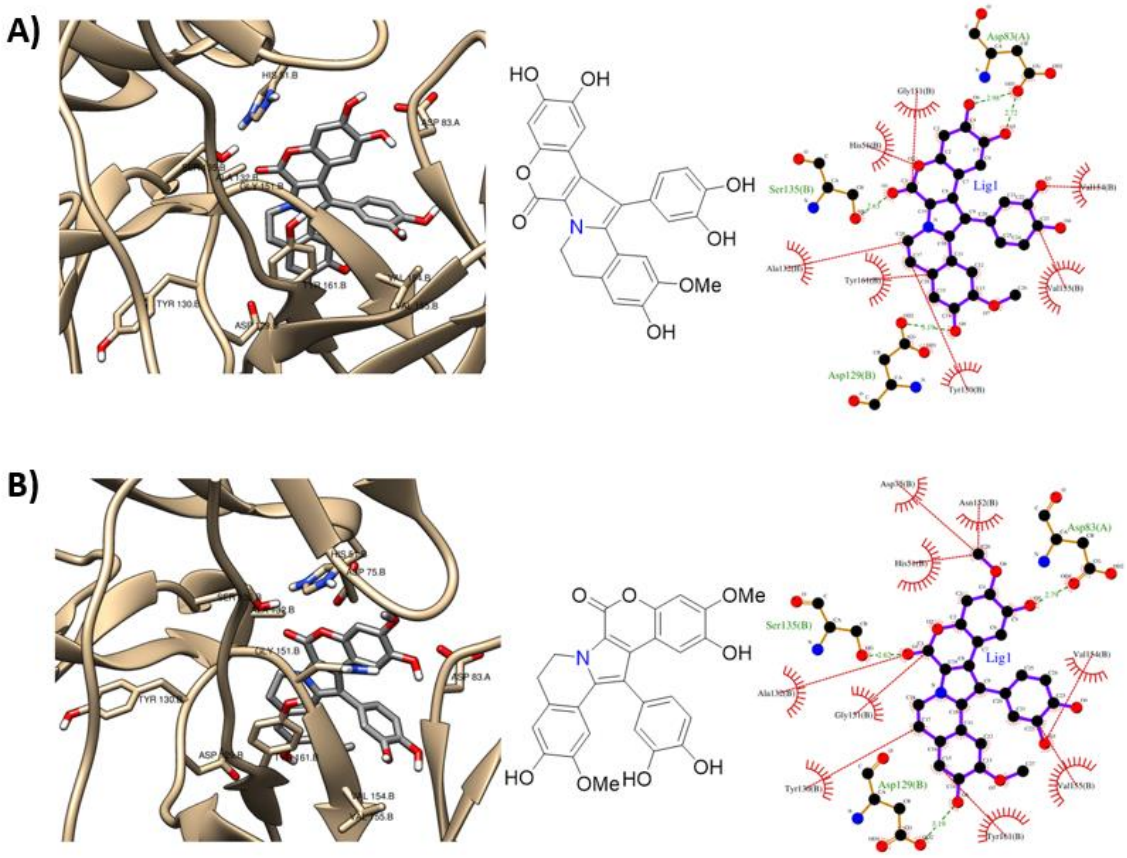

Figure 7. Interaction profiles of the best-docked poses: (**A**) for lamellarin S (**26**) and (**B**) lamellarin Z (**39**).

The 8-OH (ring A), C=O (ring D) and 21-OH (ring E) of lamellarin derivatives apparently participate in hydrogen-bonding interactions with the side chains of Asp129, Ser135 and Asp83 of the Zika MMpro enzyme, respectively, as can be seen in lamellarin S (**26**) and lamellarin Z (**39**) (**Figure 7)**. Also very relevant are the hydrophobic interactions of the ring F with the Val154 and Val155 residues of the enzyme. Other relevant hydrophobic interaction is between the ring B and Tyr130 residue of the enzyme. As with the SARS-CoV-2 Mpro enzyme, the double bond between C5 and C6 in ring B appear to be not essential for activity against Zika Mpro. In **Tables 2 and 3**, the hydrogen bond and hydrophobic interactions for the 39 lamellarin derivatives (**1-39**) in molecular docking on the targets, SARS-CoV-2 Mpro and Zika Mpro, respectively are shown.

Table 2. The detailed interactions established upon docking the (**O6K**), and lamellarin derivatives (**1**-**39**) against the SARS-CoV-2 Mpro (PDB ID: 6LU7) chain A.

Lamellarins	**Common amino acids (aa)**		**Common aa number**
	H-bond residues	**Hydrophobic interaction residues**	
F (**11**), J (**16**), N (**24**), T 20-sulfate (**29**)	none	Gln189, Glu166, His163, His164, Leu141, Met165, Phe140	7
B (**2**), B 20-sulfate (**3**), D triacetate (**8**)	Gly143	Arg188, Asn142, Cys145, Gln189, Glu166, His41, His164, Met165, Pro168, Thr190	11
I (**15**)	His41	Arg188, Asn142, Cys145, Gln189, Glu166, Gly143, His164, Leu141, Met165, Phe140, Pro168, Thr190	NA[a]
E (**9**), E 20-sulfate (**10**), L (**20**), U (**30**), U 20-sulfate (**31**), W (**34**), V 20-sulfate (**33**)	HIS163	Arg188, Asn142, Asp187, Cys145, Gln189, Glu166, Gly143, His41, Met165	10
G (**12**)	Asn142, His163	Arg188, Asp187, Cys145, Gln189, Glu166, Gly143, His41, Met49, Met165	NA[a]
D (**7**)	Asn142, Leu141	Arg188, Asp187, Gln189, Glu166, His41, His163, His164, Met165, Phe140	NA[a]
K triacetate (**19**), L triacetate (**21**), L 20-sulfate (**22**), N triacetate (**25**), T diacetate (**28**), X triacetate (**36**)	Cys145, His41	Arg188, Asn142, Gln189, Glu166, Gly143, His164, Leu141, Met49, Met165, Phe140, Pro168	13
K diacetate (**18**)	Cys145, Ser144	Arg188, Asn142, Asp187, Gln189, Glu166, Gly143, His41, His164, Leu141, Met49, MetT165, Phe140, Tyr54	NA[a]
Y 20-sulfate (**38**)	Cys145, Thr190	Ala191, Gln189, Glu166, His163, His164, Leu141, Met165, Phe140, Pro168	NA[a]
V (**32**)	Glu166, His163	Arg188, Asn142, Asp187, Cys145, Gln189, Gly143, His41, His164, Leu141, Leu167, Met165	NA[a]
A (**1**)	Gly143, Glu166	Arg188, Asn142, Asp187, Gln189, His41, His164, Leu141, Leu167, Met165	NA[a]
C (**4**)	Gly143, Leu141	Arg188, Asn142, Asp187, Gln189, Glu166, His41, His163, His164, Met165, Phe140	NA[a]
K (**17**)[c]	Gly143, Ser144	Arg188, Asn142, Asp187, Cys145, Gln189, Glu166, His41, His163, His164, Leu141, Met49, Met165	NA[a]
M (**23**)	Gly143, Thr190	Arg188, Asn142, Cys145, Gln189, Glu166, His41, His164, Met165, Phe140, Pro168	NA[a]
X (**35**)	Arg188, Gly143, Thr190	Asn142, Cys145, Gln189, Glu166, His41, His164, Met165, Pro168	NA[a]

G 8-sulfate (**13**)	Asn133, Leu287, Lys137	Arg131, Asn238, Asp197, Asp289, Leu272, Leu286, Thr199, Tyr239, Val171	NA[a]
S (**26**)[c], Z (**39**)[3]	Cys145, Gly143, Ser144	Asn142, Gln189, Glu166, His41, His163, His164, Leu141, Met49, Met165	12
C diacetate (**5**), C 20-sulfate (**6**)	Cys145, Ser144, Tyr54	Arg188, Asn142, Asp187, Gln189, Glu166, Gly143, His164, Leu141, Met49, Met165	13
T (**27**), Y (**37**)	Gly143, His41, Thr190	Arg188, Asn142, Asp187, Cys145, Gln189, Glu166, His164, Leu141, Met49, Met165, Ser144, Thr25	15
H (**14**)[3]	Asn142, Gly143, His163, Ser144	Asp187, Cys145, Gln189, Glu166, His41, His164, Leu141, Met165	NA[a]
O6K[b]	Gln189, Glu166, Tyr54	Asn142, Asp187, Cys145, His41, His163, His164, Met49, Met165, Phe140, Thr190	NA[a]

[a] Not applicable. [b] Positive Control. [c] Best docking scored molecules.

Table 3. The detailed interactions established upon docking the (**O6K**), and lamellarin derivatives (1-39) against the Zika Mpro (PDB ID: 5H4I) chains A and B.

Lamellarins	Common amino acids (aa)		Common aa number
	H-bond residues	Hydrophobic interaction residues	
B 20-sulfate (**3**), N triacetate (**25**), U 20-sulfate (**31**)	none	Ala132, Asp129, Gly151, Gly153, Ser135, Tyr130, Tyr161, Val155	8
T 20-sulfate (**29**)	Ala132, Gly153, Tyr161	Asn152, Asp83[a], HisS51, Phe84[a], Pro131, Tyr130, Val155	NA[b]
H (**14**)[d]	Asn152, Gly151, Gly153, Pro131, Tyr130	Ala132, Ser135, Tyr161, Val155	NA[b]
K diacetate (**18**)	Asp129	Ala132, Asn152, Asp75, Asp83[a], Gly151, Gly153, His51, Phe84[a], Tyr130, Tyr161, Val154, Val155	NA[b]
E 20-sulfate (**10**)	Asp129, His51, Lys54, Ser135	Ala132, Asp83[a], Tyr161, Val155	NA[b]
A (**1**), C (**4**), I (**15**), V (**32**)	Asp129, His51, Ser135, Tyr130	Ala132, Asp83[a], Gly151, Tyr161, Val155	9
E (**9**), F (**11**)	Asp129, Val155	Ala132, Asn152, Asp83[a], Gly151, His51, Ser135, Tyr130, Tyr161, Val154	11
V 20-sulfate (**33**)	Asp83[a]	Ala132, Asp129, Gly151, His51, Pro131, Ser135, Tyr130, Tyr161, Val154, Val155	NA[b]
D (**7**), N (**24**)	Asp83[a], Asp129, His51, Ser135	Ala132, Gly151, Gly153, Tyr130, Tyr161, Val154, Val155	11
K (**17**)	Asp83[a], Asp129, His51, Ser135, Tyr130	Ala132, Gly151, Gly153, Tyr161, Val154, Val155	NA[b]
J (**16**), L (**20**), G (**12**)[d], S (**26**)[d], Z (**39**)[d]	Asp83[a], Asp129, Ser135	Ala132, Gly151, His51, Tyr130, Tyr161, Val154, Val155	10
G 8-sulfate (**13**), U (**30**)	Asp83[a], Ser135	Ala132, Asn152, Asp129, GLY151, His51, Tyr130, Tyr161, Val154, Val155	11
M (**23**), X (**35**)	Asp83[a], Ser135, Tyr130	Ala132, Asn152, Asp129, Gly151, Tyr161, Val154, Val155	10
B (**2**), W (**34**)	Asp83[a], Ser135, Val155	Ala132, Asn152, Asp129, Gly153, Tyr130, Tyr161, Val154	10
Y 20-sulfate (**38**)	Gly151	Ala132, Asn152, Asp129, Gly151, Tyr130, Tyr161, Val154	NA[b]
O6K[c]	Asp83[a], Asn152, Gly153, His51, Ser135, Tyr161	Ala132, Gly151, Lys54, Ser81[a], Trp50, Val36, Val72	NA[b]

[a] From chain A. [b] Not applicable. [c] Positive Control. [d] Best docking scored molecules.

3.2 Molecular Dynamic Simulations (MDS)

3.2.1 SARS-CoV-2 Mpro

The Root Mean Square Deviation (RMSD) of both the protein and the ligand was calculated for both complexes to assess their stability by fitting them to the starting structure's backbone. **Figure 8 (A/B)** shows the protein and ligand RMSD, respectively. SARS-CoV-2 Mpro showed rapid convergence to stability complexed with lamellarin H (**14**) after ~ 10 ns and maintained an RMSD within 1 Å, indicating the stability of the complex. The RMSD of the ligand, lamellarin H (**14**), shows stability as well with an RMSD within ~ 1 Å with minor disruptions within a range of 3 Å.

On the contrary, the SARS-Cov-2 Mpro showed a significant perturbation after about 10ns when complexed with lamellarin K (**17**), which corresponds to the detachment of the ligand from the pocket due to instability. This was also confirmed by visualizing the trajectories using virtual molecular dynamics (VMD) and investigating the ligand's RMSD, which showed extreme instability and substantial deviation, indicating the loose motion of the ligand in the system unbounded to the protein[104]. Regarding any further analyses, the lamellarin K (**17**)-Mpro complex will be ignored.

For further stability analysis, we investigated the compactness of the protein by calculating its radius of gyration (Rg). Basically, we are investigating the distribution of protein atoms from their centre of mass, which will give us a direct indication of the folding and the stability of the protein. SARS-CoV-2 Mpro showed consistent compactness when complexed lamellarin H with a slight increase in compactness for some instances throughout the simulation, indicating the overall structural stability of the complex, as shown in **Figure 8 (C)**.

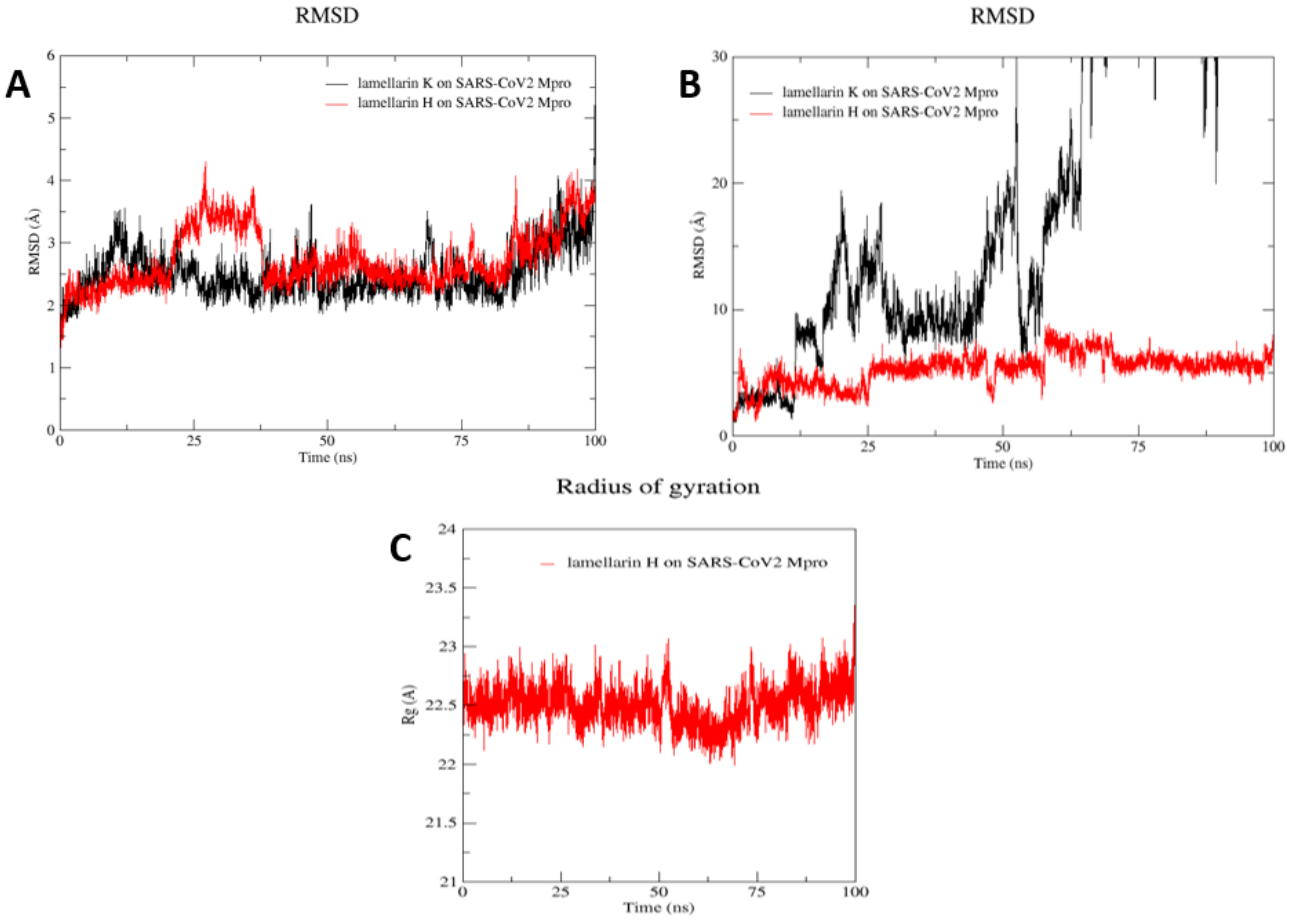

Figure 8: (**A**) the protein RMSD of SARS-CoV-2 bound to Lamellarins H/K (**14**/**17**). (**B**) the ligands' RMSD. (**C**) the radius of gyration of the SARS-CoV-2 M^{pro} bound to lamellarin H (**14**)

3.2.2 Binding Analysis and Free Energy Calculations of lamellarin H (14) Bound to SARS-CoV-2 Mpro

To understand the mode of binding of Lamellarin H and assess its affinity, we carried out a hydrogen bond analysis to investigate the capability of the compound to elicit and maintain different hydrogen bonds within the pocket. The cutoff distance for the hydrogen bonds was set to 3.5 Å while the cutoff angle was 30°. Our ligand maintained five hydrogen bonds within the pocket of SARS-CoV2 Mpro throughout the simulation once it converged to stability ~ 10 ns, as shown in **Figure 9 (B)**. we also investigated the total contacts experienced by Lamellarin H throughout the 100ns with a 3 Å distance cutoff. **Figure 9 (A)** shows the total contacts plotted against the time in nanoseconds, showing Lamellarin H experiencing an average of ~ 20 contacts.

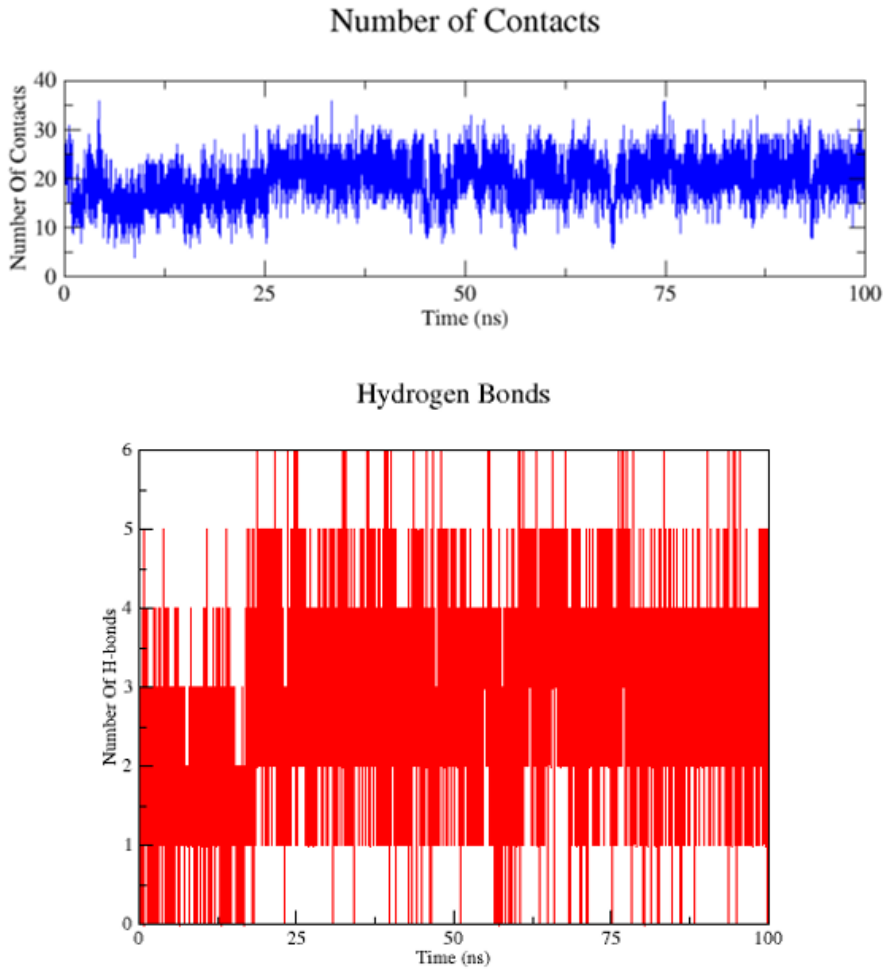

Figure 9: (**A**) the total contacts experienced by lamellarin H (**14**) plotted against time in nanoseconds. (**B**) the number of hydrogen bonds maintained by lamellarin H (**14**) throughout the simulation.

Indeed, for a more robust binding affinity assessment, we ran free energy calculations for the complex along with a decomposition analysis for the residues within 6 Å from the ligand to indicate the high interacting pocket residues responsible for the possible inhibition activity of the lamellarin H (**14**). the following (**Table 3**) shows the calculated different energy terms with the total free energy term calculated for Lamellarin H bound to SARS-CoV-2 Mpro. Those values are also plotted in **Figure 10 (A)**.

Table 3: The free energy components calculated for the lamellarin H (**14**)-SARS-CoV-2 complex.

VDWAALS (Kcal/mol)	EEL (Kcal/mol)	EPB (Kcal/mol)	ENPOLAR (Kcal/mol)	GGAS (Kcal/mol)	GSOLV (Kcal/mol)	TOTAL (Kcal/mol)
-32.3	-31.61	48.83	-3.63	-63.91	45.2	-18.71

Through the energy decomposition analysis, six residues within the pocket were indicated to be highly interacting with lamellarin H (**14**). These residues are ASN142, GLU166, ASP187, ARG188, GLN189, and GLN 192. Furthermore, their energy contributions, along with the other residues within 6 Å from the ligand are plotted in **Figure 10 (B)**, and as a heatmap in **Figure 10 (C)** where their energy contributions are plotted against time represented in the simulation's frames. **Figure 10 (D)** gives a 3D representation of lamellarin H (**14**) binding mode with these residues using the same colour code used for the heatmap. Based on the previous analysis and lamellarin H (**14**) having a total change in the binding free energy to SARS-CoV-2 of -18.71 Kcal/mol, indicating a spontaneous process, we are encouraged to propose lamellarin H (**14**) as a potential SARS-CoV-2 M^{pro} inhibitor.

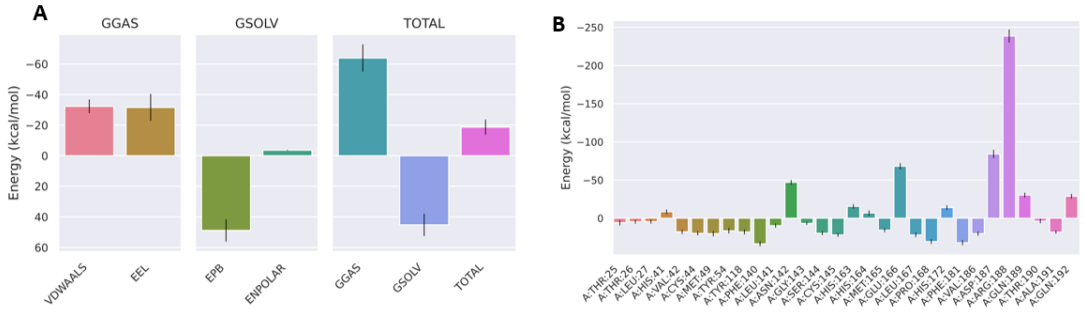

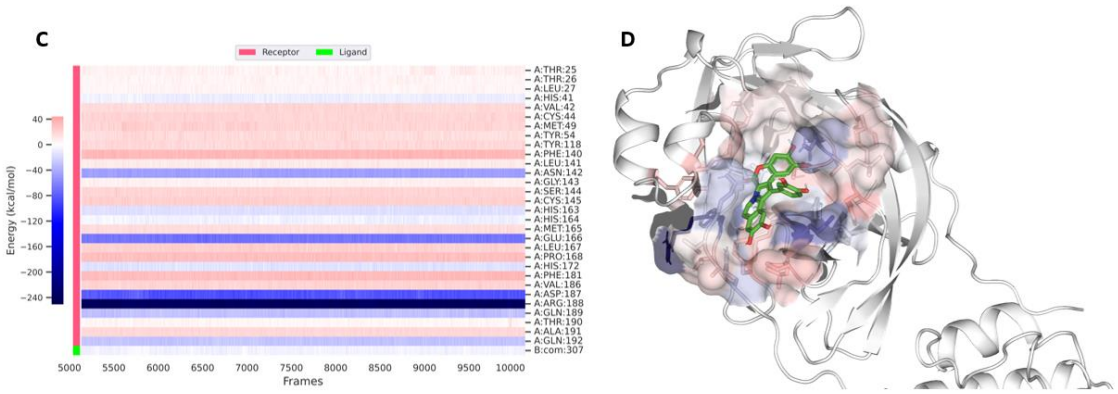

Figure 10: (**A**) The free energy components of Lamellarin H bound to SARS-CoV-2 M^{pro}. (**B**) The individual residue's energy contributions. (**C**) A heatmap shows the energy contribution of individual residues plotted against time. (**D**) A 3D visualization of lamellarin H (**14**) mode of binding with colors corresponding to the heatmap.

3.2.3 Zika Mpro

Regarding the Zika virus Mpro, the top two performing compounds in molecular docking were lamellarin S (**26**) and lamellarin Z (**39**). Both were simulated for 100 ns, each complexed with the Zika Mpro, to perform advanced analysis of binding affinity and complex stability. Both complexes showed excellent stability once they converged after about 15 ns. Both RMSD were within 1 Å, with Zika M^{pro} showing slightly minor perturbations when complexed with lamellarin Z (**39**) compared to lamellarin S (**26**). However, both showed excellent stability, which was also confirmed by the ligand RMSDs, which showed excellent stability of both ligands. However, lamellarin S (**26**) showed more robust stability once converged, ~ 25 ns, with fewer disruptions than lamellarin Z (**39**), which showed stability almost since the beginning of the simulation but converged to more structural stability in the second half of the simulation. The protein's RMSD and the ligands' RMSD are shown in **Figure 11 (A/B)**, respectively.

We also calculated the radius of gyration of the protein in both systems to investigate the compactness of the protein. Consequently, Zika Mpro bound to lamellarin Z (**39**) showed more significant disturbances in the Rg, as shown in **Figure 11 (C)** ; However, both systems showed consistent Rg after around 25 ns, corresponding to the complexes converging to stability. Based on that, we can confirm the overall structural stability of Zika Mpro when it is bound to lamellarins S (**26**) and Z (**39**), with more stability observed in the case of lamellarin S (**26**)

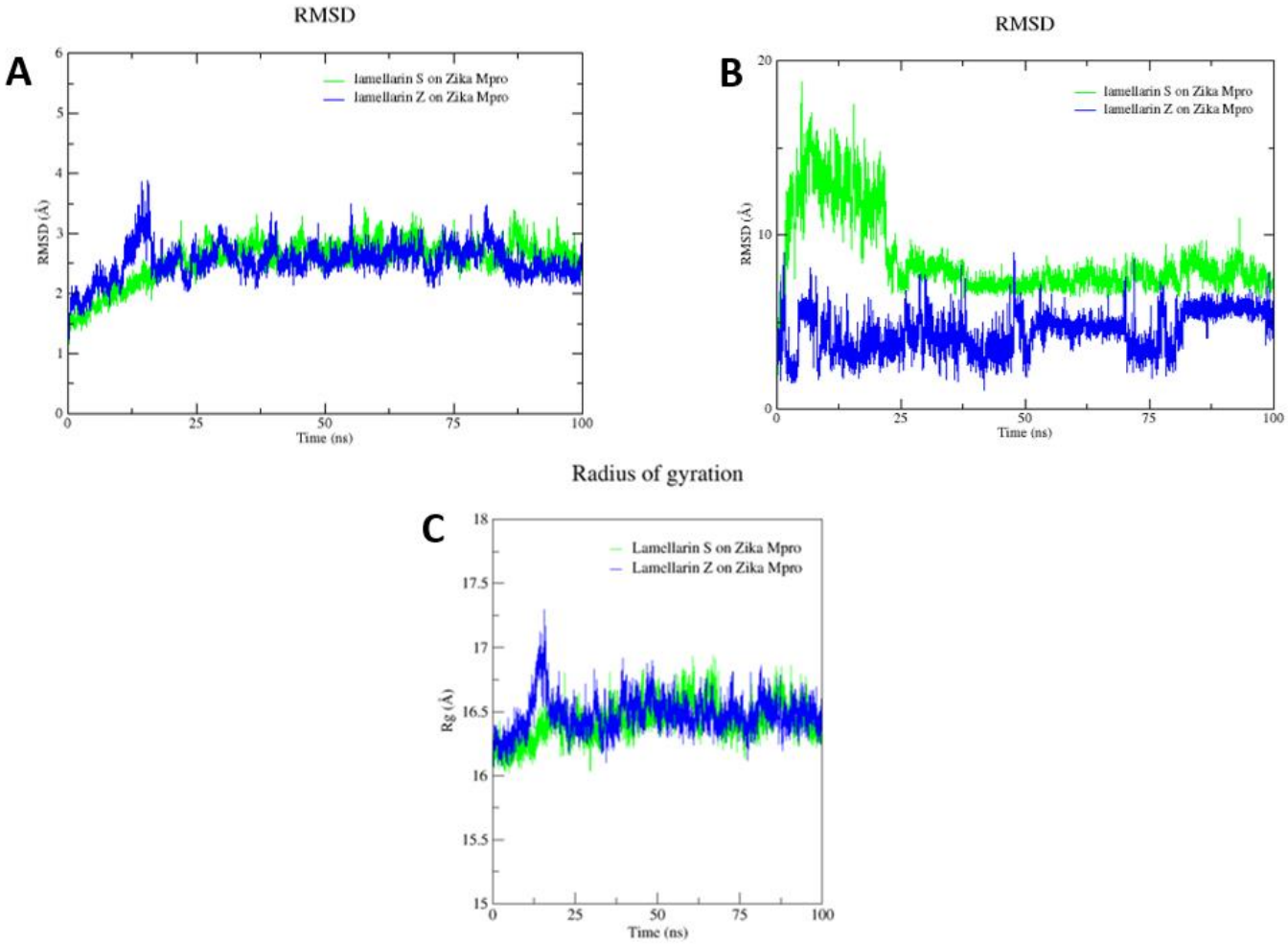

Figure 11: (**A**) the protein RMSDs for Zika Mpro bound to lamellarin S and Z (**26**)/(**39**). (**B**) the Ligands' RMSDs. (**C**) the Radius of Gyration of the protein

3.2.4 Binding Analysis and Free Energy Calculations of Lamellarins S/Z (26/39) Bound to Zika Mpro

Similarly, a total contacts analysis along with hydrogen bond analysis were carried out for both lamellarin S (**26**) and lamellarin Z (**39**). As shown in **Figure 12 (A)**, lamellarin S (**26**) was found to maintain a higher number of contacts with Zika Mpro with an average of ~ 17 contacts than lamellarin Z (**39**), which had an average total of around 14 contacts. It is easy to visually notice the increasing number of lamellarin S (**26**)'s contacts starting from ~ 25 ns till it reached the highest starting from ~ 40 ns, then it maintained those contacts once it reached complete stability within the pocket for the rest of the simulation. Regarding the hydrogen bond analysis, lamellarin S (**26**) could maintain about four to five hydrogen bonds once it reached complete stability (at ~ 40ns). On the contrary, lamellarin Z (**39**) could not preserve that much. It could maintain only two hydrogen bonds throughout most of the simulation, as shown in **Figure 12 (B)**.

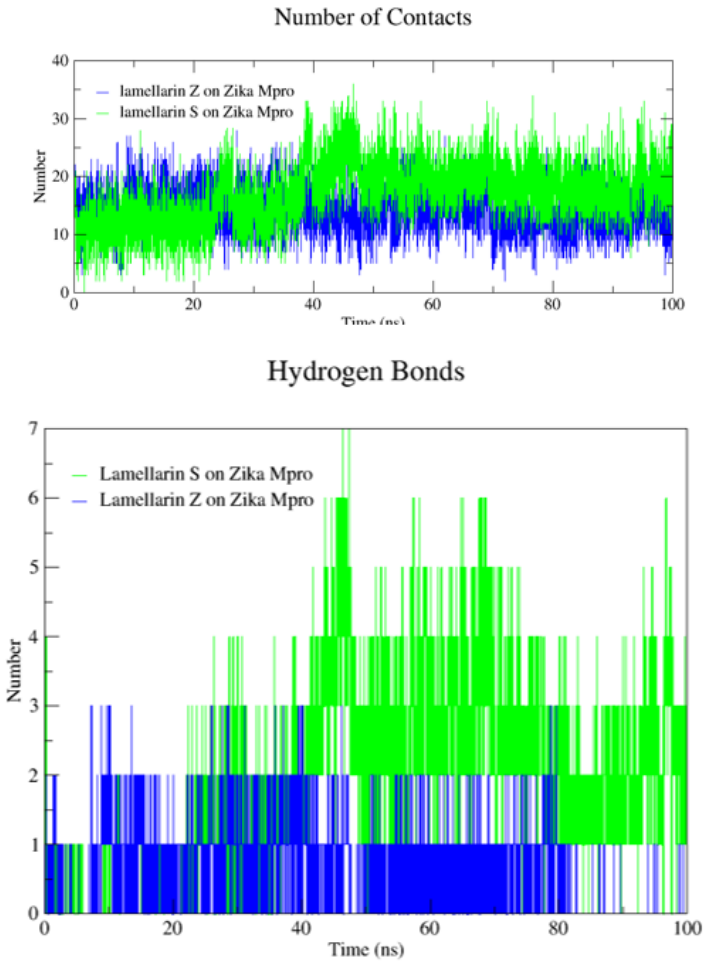

Figure 12: (**A**) Total contacts experienced by both lamellarins S/Z (**26**/**39**) within the Zika Mpro pocket. (**B**) Hydrogen bonds maintained by both compounds

The free energy calculations came consistent with the previous observations, showing that lamellarin S (**26**) has a substantially higher binding affinity compared to Lamellarin Z (**39**). Lamellarin S (**26**) was found to have a total change in free energy of -25.18 Kcal/mol compared to -12.25 Kcal/mol observed for lamellarin Z (**39**). **Table 4** contains all the calculated energy components which are also plotted for both compounds in **Figure 13 (A/B)**.

Table 4: The free energy components calculated for both lamellarins S/Z (**26**/**39**)

Compound	VDWAALS (Kcal/mol)	EEL (Kcal/mol)	EPB (Kcal/mol)	ENPOLAR (Kcal/mol)	GGAS (Kcal/mol)	GSOLV (Kcal/mol)	TOTAL (Kcal/mol)
Lame. S (**26**)	-34.86	-20.1	33.39	-3.61	-54.96	29.78	-25.18
Lame. Z (**36**)	-25.49	-10.6	27.03	-3.19	-36.09	23.84	-12.25

We verified through the energy decomposition analysis that both compounds could interact strongly with ASP83, ASP75, ASP129, ASN152, and HIS51, as shown in **Figure 13 (C/D)** . However, it was noticed that lamellarin Z (**39**) had much more unfavourable interactions with the other residues, especially TRP50 and SER81, with which lamellarin S (**26**) showed no unfavourable interactions.

This can be easily observed in the individual residues' energy contribution graphs [**Figure 13 (C/D)**] and the heatmaps showing the individual energy contribution through the simulation's timeline [**(Figure 13 (E/F)**]. Consequently, lamellarin S (**26**) is found to fit the pocket cavities vastly superior to lamellarin Z (**39**), interpreting the previous remarks. The 3D binding pose represented using the same colour code used for the heatmaps for both compounds is shown in **Figure 13 (G/H)**.

Thus, we anticipate lamellarin S (**26**) to have excellent potential as an antiviral for the Zika virus by targeting its main protease (Mpro)

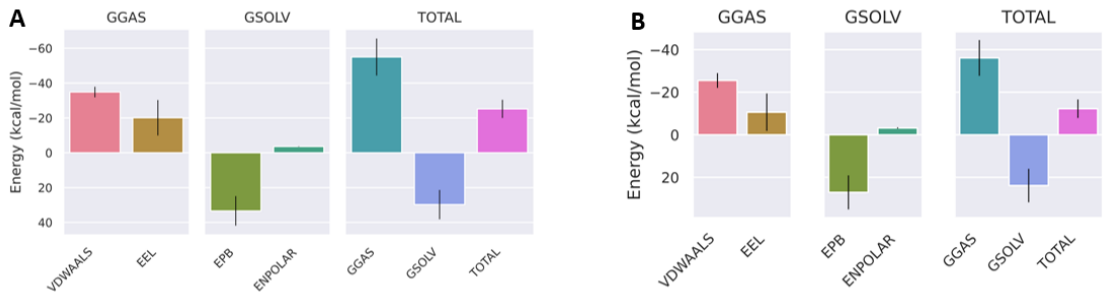

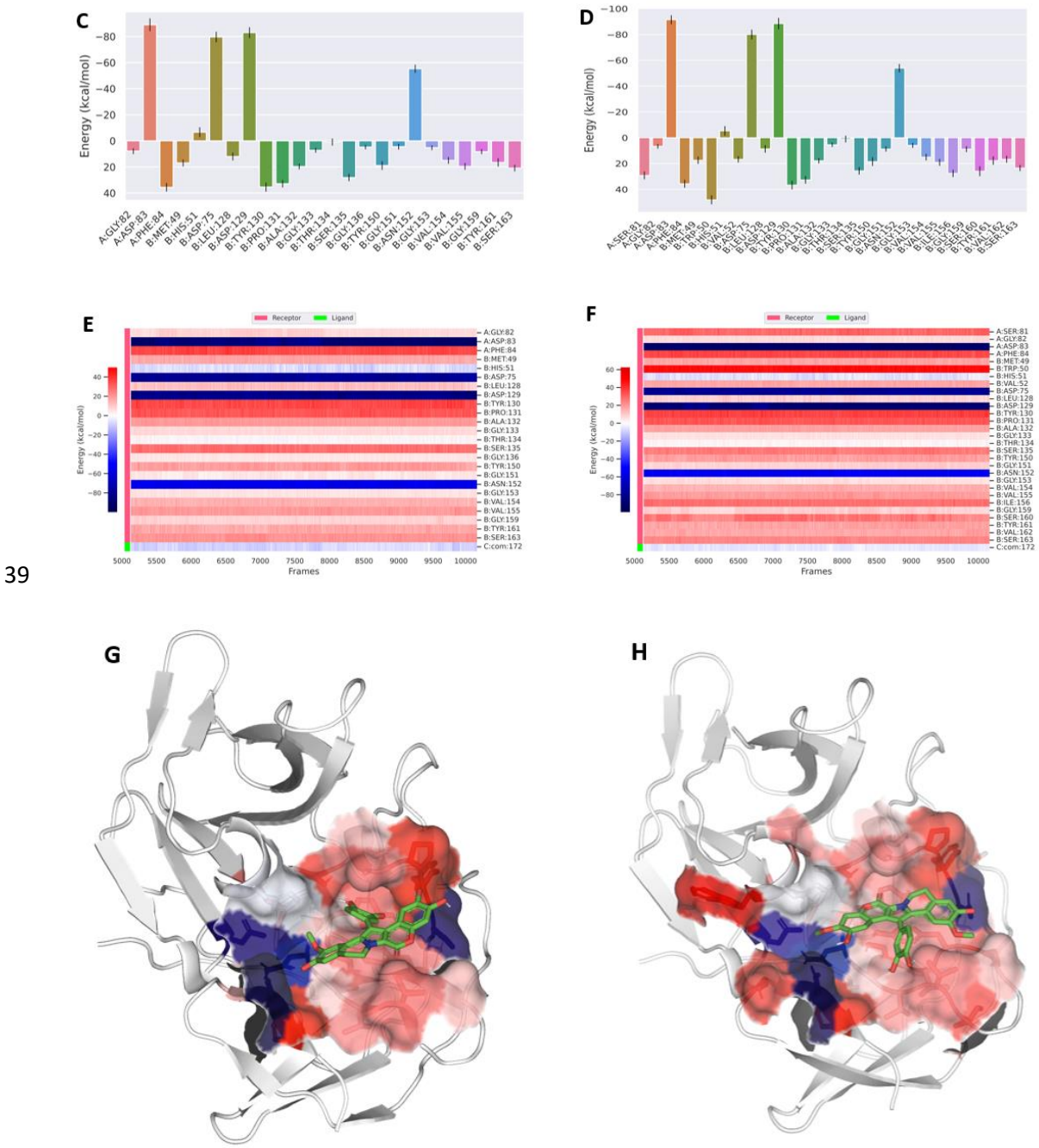

Figure 13: (**A**) the free energy components of lamellarin S (**26**) bound to Zika Mpro. (**B**) the energy components for lamellarin Z (**39**). (**C**) the individual residue's energy contributions for lamellarin S (**26**). (**D**) the individual residue's energy contributions for lamellarin Z (**39**). (**E**) heatmap shows the energy contribution of individual residues plotted against time for lamellarin S (**26**). (**F**) the heatmap for lamellarin Z (**39**). (**G**) 3D visualization of lamellarin S (**26**) bound to Zika Mpro. (**H**) 3D visualization of lamellarin Z (**39**).

3.3. *In Silico* Prediction of Pharmacokinetics, Toxicity and Druglikeness (ADME/Tox)

In order to assess our compounds' pharmacokinetics, SwissADME, an online free tool, was used to evaluate the compounds' properties. It was found that lamellarins H/K (**14**/**17**) had only 1 Lipinski rule violation each, while lamellarin H (**14**) also had one Veber's rule violation and one PAINS alert (**Table 5**). Moreover, lamellarins S/Z (**26**/**39**) had one PAINS alert and one Veber's rule violation for lamellarin S (**26**). The four compounds had expected low GI absorption, and no blood-brain barrier penetration was predicted for any of them.

Table 5: ADME/Tox profiling of four selected lamellarins compounds

Compound	Lipinski #violations	Veber #violations	PAINS #alerts	GI absorption	BBB permeant
Lamellarin H (**14**)	1	1	1	Low	No
Lamellarin K (**17**)	1	0	0	Low	No
Lamellarin S (**26**)	0	1	1	Low	No
Lamellarin Z (**39**)	0	0	1	Low	No

3.4. Structure-Activity Relationship Studies (SARs)

Structurally, most of the lamellarins isolated possess a fused benzopyrano-pyrrolo-isoquinolinone hybrid ring system as a common scaffold as shown in (**Figure 14**). Extensive analysis of the 39 lamellarins marine alkaloids under investigation, indicated that, the aromatic A-, E-, and F-rings are densely decorated either by hydroxy or methoxy groups. Additionally, in eight lamellarin derivatives, the A-, E-, and F-rings are also decorated by acetyl groups. Moreover, there are as further nine lamellarin derivatives that possess a sulfonyl group in the A- or E-ring. The 5,6-bond in ring D can be either saturated or unsaturated.

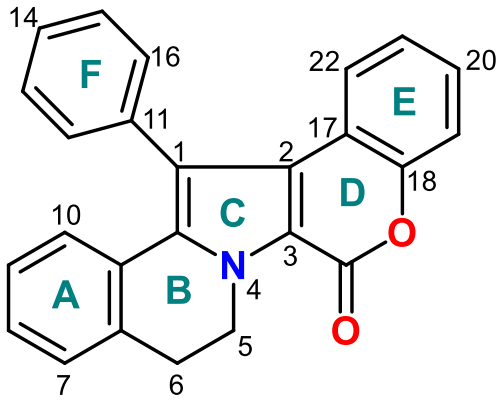

Figure 14. Polycyclic core of the lamellarin-derived pyrrole marine alkaloids

In the SARS-CoV-2 Mpro activity of lamellarin derivatives, the existence of a hydroxyl group at position 14 of the ring F, that can exchange with position 13 in the same ring, appears to be essential. For the ten selected lamellarin derivatives for SARS-CoV-2 Mpro reported in **Table 1**, only lamellarin J (**16**) does not follow this rule. Furthermore, the hydrophobic engagement by the F and A rings to the SARS-CoV-2 Mpro enzyme in reference amino acids such as Cys145 and His41, respectively, also seems very relevant. The same behavior was observed for the positive control, (**O6K**), with the SARS-CoV-2 Mpro in (**Figure 4A)** by the benzyl and γ-lactam moieties. Contrary to what has been reported for anti-HIV activity [105], the presence of sulfate groups does not appear to have relevance for activity against SARS-CoV-2 Mpro. As can be seen by the ΔG_B calculated values for the lamellarin derivative B (**2**) and B 20 sulfate (**3**) of -8.13 Kcal/mol and -8.40 Kcal/mol (Table S1 of the *Supplementary Data*), respectively. For the nine sulfonated lamellarin derivatives, it appears that the absolute deviation between the ΔG_B of the sulfonated derivatives and the ΔG_B of the corresponding non-sulfonated derivatives varies from 0.57 Kcal/mol [G (**12**) and G 8-sulfate (**13**)] to 0.07 Kcal/mol [V (**32**) and V 20-sulfate (**33**)] (**Chart 1**). Concerning the Zika Mpro, the activity of lamellarin derivatives is mainly dependant on the existence of a hydroxyl group at position 21 of the ring E, that can exchange with position 20 in the same ring, and a δ-lactone ring (ring D) appear to be essential. For the ten selected lamellarin derivatives against Zika Mpro reported in Table 1, only lamellarin L 20-sulfate (**22**) does not featuring a hydroxyl group at position 21 or 20 of the ring E. The positive control (**O6K**), showed a similar behaviour with Zika Mpro enzyme (**Figure 4B**) in the hydroxyl group and in the δ-lactone ring, respectively (**Chart 2**).

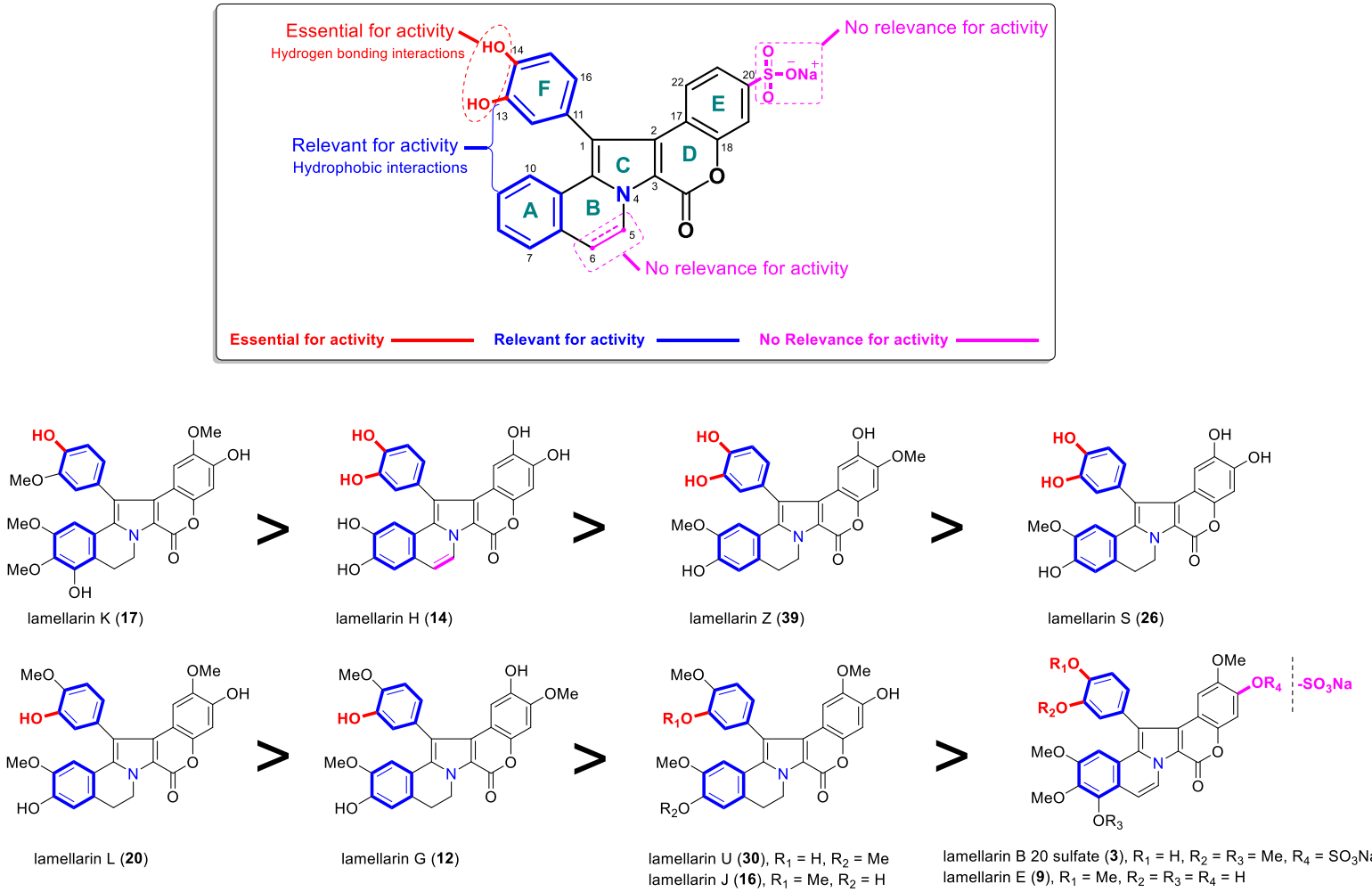

Chart 1: SARs studies for most promising lamellarins compounds against SARS-Cov-2 Mpro based on their binding affinities values and compered to positive control (**OK6**)

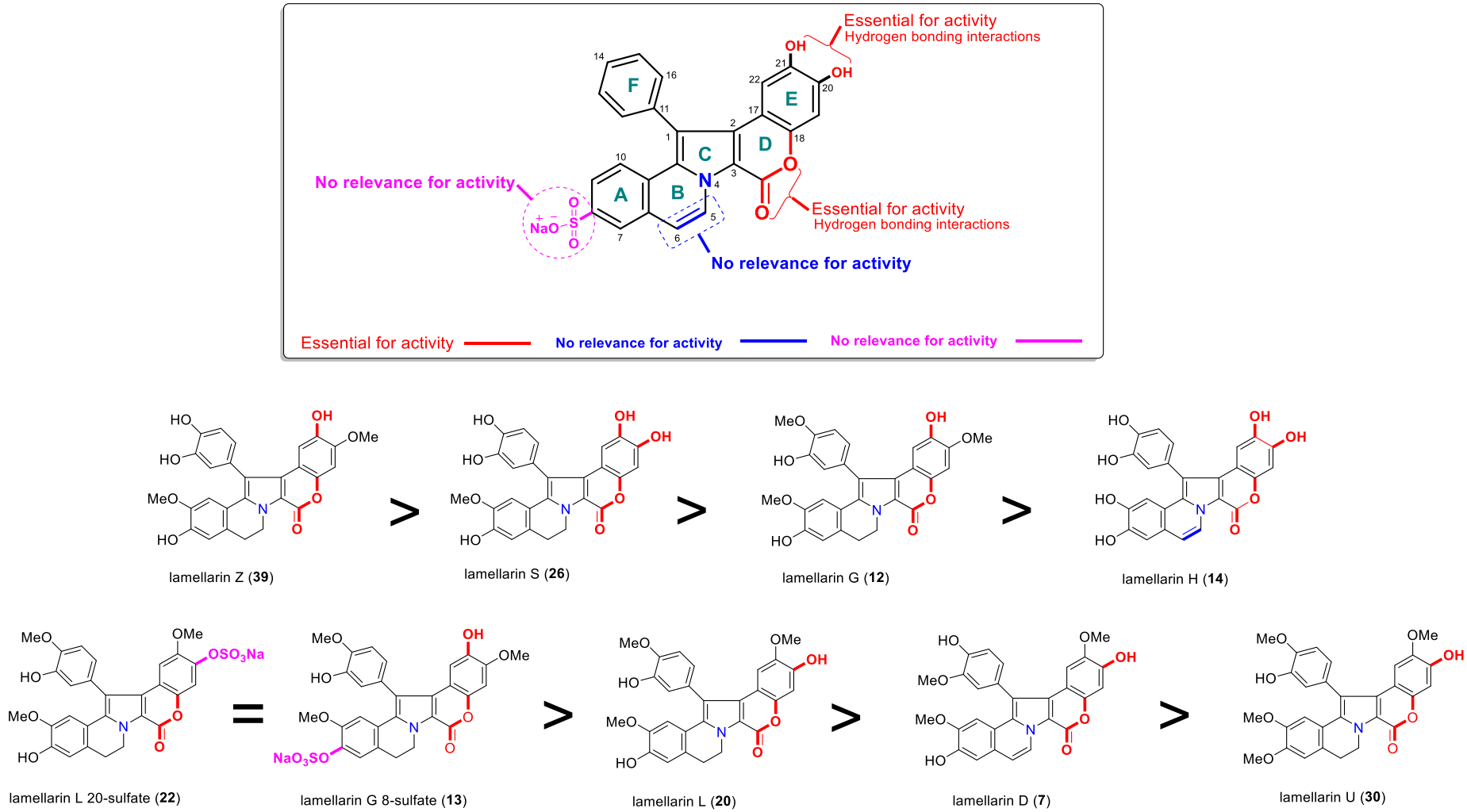

Chart 2: SARs studies for most promising lamellarins compounds against Zika Mpro based on their binding affinities values and compered to positive control (**OK6**)

4. Conclusion and Prospective

Alongside the highly expressed global effort to identify either synthetic or natural potential antivirals, in this communication, a focused chemical library of 39 marine polycyclic lamellarin pyrrole alkaloids (**LPAs**) were comprehensively investigated for their binding affinities against SARS-CoV-2 and Zika main proteases (Mpro) using an integrated set of computational means including molecular docking (MDock), molecular dynamic simulations (MDS) and structure activity relationships (SARs) studies. Indeed, MDock simulation studies showed that most of the investigated marine compounds are demonstrating very interesting binding scores particularly, four compounds namely, [lamellarin H (**14**)/lamellarin K (**17**)] and [lamellarin S (**26**)/ lamellarin Z (**39**)], which were identified as potential antiviral hits for hunting SARS-CoV-2 and Zika main proteases respectively, based on their prominent ligand-protein energy scores and relevant binding affinities with (Mpro) pocket residues. Meanwhile, they displayed very close binding scores compared to the co-crystallized inhibitor (**O6K**, positive control). Indeed, the MD simulations showed a noticeable stability for almost of the investigated marine compounds at the (Mpro) binding site. Furthermore, fundamental SARs investigations were conducted to link between such divergent structural characteristics and how they potentially affected the expected activity. Those encouraging findings highlighted that such distinguished molecular scaffolds are deserved and could illuminate the expansion of potential antivirals for controlling SARS-Cov-2 and Zika viruses. Moreover, considering the valid and easily accessible chemical syntheses for a numerous number of these marine compounds and their structurally related congeners, which could be encouraging for more in *vitro /in vivo* preclinical investigations [60, 106-109].

Credits of Authorship contribution

Conceptualization: Florbela Pereira, Reem K. Arafa and Amr El-Demerdash. **Validation**: Florbela Pereira, Reem K. Arafa and Amr El-Demerdash. **Formal analysis**: Florbela Pereira, Reem K. Arafa and Amr El-Demerdash. **Investigation**: Florbela Pereira, Loay Bedda, Mohamed A. Tammam, Abdul Kader Alabdullah, Reem K. Arafa and Amr El-Demerdash. **Resources**: Florbela Pereira, Loay Bedda, Mohamed A. Tammam, Abdul Kader Alabdullah, Reem K. Arafa and Amr El-Demerdash. **Data curation**: Florbela Pereira, Reem K. Arafa and Amr El-Demerdash. **Writing original draft**: Florbela Pereira, Loay Bedda, Mohamed A. Tammam, Abdul Kader Alabdullah, Reem K. Arafa and Amr El-Demerdash. **Writing-review & editing**: Florbela Pereira, Loay Bedda, Mohamed A. Tammam, Abdul Kader Alabdullah, Reem K. Arafa and Amr El-Demerdash.

Declaration of competing interest

The authors declare that they have no known competing financial interests or personal relationships that could have appeared to influence the work reported in this paper.

Funding

Amr El-Demerdash is immensely grateful to the John Innes Centre, Norwich Research Park, United Kingdom for the postdoctoral fellowship. Florbela Pereira would like to thank Fundacão para a Ciência e a Tecnologia, MCTES, in the scope of the project UIDB/50006/2020 of the Research Unit, Associate Laboratory for Green Chemistry, LAQV".

Acknowledgments

Amr El-Demerdash is immensely grateful to his home university, Mansoura University, Egypt for the unlimited support inside and outside.

References

[1] J. Louten, Virus Replication, in: Essential Human Virology, Elsevier, 2016, pp. 49-70.

[2] K.H. Choi, Viral polymerases, Adv. Exp. Med. Biol., 726 (2012) 267-304.

[3] J. Zephyr, N. Kurt Yilmaz, C.A. Schiffer, Viral proteases: Structure, mechanism and inhibition, Enzymes, 50 (2021) 301-333.

[4] J.S.Y. Ho, Z.Y. Zhu, I. Marazzi, Unconventional viral gene expression mechanisms as therapeutic targets, Nature, 593 (2021) 362-371.

[5] T.E. Schlub, E.C. Holmes, Properties and abundance of overlapping genes in viruses, Virus Evol, 6 (2020).

[6] J. Sztuba-Solinska, V. Stollar, J.J. Bujarski, Subgenomic messenger RNAs: Mastering regulation of (+)-strand RNA virus life cycle, Virology, 412 (2011) 245-255.

[7] W.D. Penn, H.R. Harrington, J.P. Schlebach, S. Mukhopadhyay, Regulators of Viral Frameshifting: More Than RNA Influences Translation Events, Annu Rev Virol, 7 (2020) 219-238.

[8] A.E. Firth, I. Brierley, Non-canonical translation in RNA viruses, J. Gen. Virol., 93 (2012) 1385-1409.

[9] Z.T. Lv, Y. Chu, Y. Wang, HIV protease inhibitors: a review of molecular selectivity and toxicity, Hiv Aids-Res Palliat, 7 (2015) 95-104.

[10] C. Lin, HCV NS3-4A Serine Protease, in: S.L. Tan (Ed.) Hepatitis C Viruses: Genomes and Molecular Biology, Horizon Bioscience, Norfolk (UK), 2006.

[11] E.Z.K. Cheong, J.P. Quek, L. Xin, C. Li, J.Y. Chan, C.W. Liew, Y. Mu, J. Zheng, D. Luo, Crystal structure of the Rubella virus protease reveals a unique papain-like protease fold, J. Biol. Chem., 298 (2022) 102250.

[12] A. Castello, E. Alvarez, L. Carrasco, The multifaceted poliovirus 2A protease: regulation of gene expression by picornavirus proteases, J. Biomed. Biotechnol., 2011 (2011) 369648.

[13] J. Steinberger, T. Skern, The leader proteinase of foot-and-mouth disease virus: structure-function relationships in a proteolytic virulence factor, Biol. Chem., 395 (2014) 1179-1185.

[14] P. Erbel, N. Schiering, A. D'Arcy, M. Renatus, M. Kroemer, S.P. Lim, Z. Yin, T.H. Keller, S.G. Vasudevan, U. Hommel, Structural basis for the activation of flaviviral NS3 proteases from dengue and West Nile virus, Nat. Struct. Mol. Biol., 13 (2006) 372-373.

[15] Q.X. Li, C.B. Kang, Structure and Dynamics of Zika Virus Protease and Its Insights into Inhibitor Design, Biomedicines, 9 (2021).
[16] R. Cannalire, C. Cerchia, A.R. Beccari, F.S. Di Leva, V. Summa, Targeting SARS-CoV-2 Proteases and Polymerase for COVID-19 Treatment: State of the Art and Future Opportunities, J. Med. Chem., 65 (2022) 2716-2746.
[17] S.P. Gupta, Viral proteases and their inhibitors, Elsevier/Academic Press, London, 2017.
[18] T.L. Blundell, S. Patel, High-throughput X-ray crystallography for drug discovery, Curr. Opin. Pharm., 4 (2004) 490-496.
[19] Y.F. Hu, K. Cheng, L.C. He, X. Zhang, B. Jiang, L. Jiang, C.G. Li, G. Wang, Y.H. Yang, M.L. Liu, NMR-Based Methods for Protein Analysis, Anal Chem, 93 (2021) 1866-1879.
[20] WHO, in.
[21] R.J. Lu, X. Zhao, J. Li, P.H. Niu, B. Yang, H.L. Wu, W.L. Wang, H. Song, B.Y. Huang, N. Zhu, Y.H. Bi, X.J. Ma, F.X. Zhan, L. Wang, T. Hu, H. Zhou, Z.H. Hu, W.M. Zhou, L. Zhao, J. Chen, Y. Meng, J. Wang, Y. Lin, J.Y. Yuan, Z.H. Xie, J.M. Ma, W.J. Liu, D.Y. Wang, W.B. Xu, E.C. Holmes, G.F. Gao, G.Z. Wu, W.J. Chen, W.F. Shi, W.J. Tan, Genomic characterisation and epidemiology of 2019 novel coronavirus: implications for virus origins and receptor binding, Lancet, 395 (2020) 565-574.
[22] A.G. Wrobel, D.J. Benton, P.Q. Xu, C. Roustan, S.R. Martin, P.B. Rosenthal, J.J. Skehel, S.J. Gamblin, SARS-CoV-2 and bat RaTG13 spike glycoprotein structures inform on virus evolution and furin-cleavage effects, Nat. Struct. Mol. Biol., 27 (2020) 763-+.
[23] F. Krammer, SARS-CoV-2 vaccines in development, Nature, 586 (2020) 516-527.
[24] C. Liu, Q.Q. Zhou, Y.Z. Li, L.V. Garner, S.P. Watkins, L.J. Carter, J. Smoot, A.C. Gregg, A.D. Daniels, S. Jervey, D. Albaiu, Research and Development on Therapeutic Agents and Vaccines for COVID-19 and Related Human Coronavirus Diseases, Acs Central Sci, 6 (2020) 315-331.
[25] S. Su, L.Y. Du, S.B. Jiang, Learning from the past: development of safe and effective COVID-19 vaccines, Nature Reviews Microbiology, 19 (2021) 211-219.
[26] R. Wang, J.H. Chen, G.W. Wei, Mechanisms of SARS-CoV-2 Evolution Revealing Vaccine-Resistant Mutations in Europe and America, J Phys Chem Lett, 12 (2021) 11850-11857.

[27] H.P. Yao, Y.T. Song, Y. Chen, N.P. Wu, J.L. Xu, C.J. Sun, J.X. Zhang, T.H. Weng, Z.Y. Zhang, Z.G. Wu, L.F. Cheng, D.R. Shi, X.Y. Lu, J.L. Lei, M. Crispin, Y.G. Shi, L.J. Li, S. Li, Molecular Architecture of the SARS-CoV-2 Virus, Cell, 183 (2020) 730-+.

[28] M.A. Shereen, S. Khan, A. Kazmi, N. Bashir, R. Siddique, COVID-19 infection: Origin, transmission, and characteristics of human coronaviruses, J Adv Res, 24 (2020) 91-98.

[29] A.R. Fehr, S. Perlman, Coronaviruses: an overview of their replication and pathogenesis, Methods Mol Biol, 1282 (2015) 1-23.

[30] Y.A. Helmy, Fawzy, M., Elaswad, A., Sobieh, A., Kenney, S. P., Shehata, A. A., The COVID-19 Pandemic: A Comprehensive Review of Taxonomy, Genetics, Epidemiology, Diagnosis, Treatment, and Control, Journal of Clinical Medicine, 9 (2020).

[31] W.Z. Yan, Y.H. Zheng, X.T. Zeng, B. He, W. Cheng, Structural biology of SARS-CoV-2: open the door for novel therapies, Signal Transduct Tar, 7 (2022).

[32] C.J. Michel, C. Mayer, O. Poch, J.D. Thompson, Characterization of accessory genes in coronavirus genomes, Virol J, 17 (2020).

[33] S. Hasan, S.F. Jamdar, M. Alalowi, S.M.A. Al Beaiji, Dengue virus: A global human threat: Review of literature, J Int Soc Prev Commu, 6 (2016) 1-6.

[34] L.R. Petersen, A.C. Brault, R.S. Nasci, West Nile Virus: Review of the Literature, Jama-J Am Med Assoc, 310 (2013) 308-315.

[35] A.R. Plourde, E.M. Bloch, A Literature Review of Zika Virus, Emerging Infect. Dis., 22 (2016) 1185-1192.

[36] C. Newman, T.C. Friedrich, D.H. O'Connor, Macaque monkeys in Zika virus research: 1947-present, Curr Opin Virol, 25 (2017) 34-40.

[37] N.M. Ferguson, Z.M. Cucunuba, I. Dorigatti, G.L. Nedjati-Gilani, C.A. Donnelly, M.G. Basanez, P. Nouvellet, J. Lessler, EPIDEMIOLOGY. Countering the Zika epidemic in Latin America, Science, 353 (2016) 353-354.

[38] S.J. Hung, S.W. Huang, Contributions of Genetic Evolution to Zika Virus Emergence, Front Microbiol, 12 (2021) 655065.

[39] D. Sirohi, R.J. Kuhn, Zika Virus Structure, Maturation, and Receptors, J. Infect. Dis., 216 (2017) S935-S944.

[40] G. Avila-Perez, A. Nogales, V. Martin, F. Almazan, L. Martinez-Sobrido, Reverse Genetic Approaches for the Generation of Recombinant Zika Virus, Viruses, 10 (2018).

147 [41] J.K. Lee, O.S. Shin, Advances in Zika Virus-Host Cell Interaction: Current
148 Knowledge and Future Perspectives, Int J Mol Sci, 20 (2019).
149 [42] W.W. Phoo, Y. Li, Z.Z. Zhang, M.Y.Q. Lee, Y.R. Loh, Y.B. Tan, E.Y. Ng, J. Lescar,
150 C.B. Kang, D.H. Luo, Structure of the NS2B-NS3 protease from Zika virus after self-
151 cleavage, Nat Commun, 7 (2016).
152 [43] Y. Shi, G.F. Gao, Structural Biology of the Zika Virus, Trends Biochem. Sci., 42
153 (2017) 443-456.
154 [44] S. Voss, C. Nitsche, Inhibitors of the Zika virus protease NS2B-NS3, Bioorganic &
155 Medicinal Chemistry Letters, 30 (2020).
156 [45] C. Nitsche, Proteases from dengue, West Nile and Zika viruses as drug targets,
157 Biophys Rev, 11 (2019) 157-165.
158 [46] A.G. Atanasov, S.B. Zotchev, V.M. Dirsch, I.E. Orhan, M. Banach, J.M. Rollinger,
159 D. Barreca, W. Weckwerth, R. Bauer, E.A. Bayer, M. Majeed, A. Bishayee, V. Bochkov,
160 G.K. Bonn, N. Braidy, F. Bucar, A. Cifuentes, G. D'Onofrio, M. Bodkin, M. Diederich,
161 A.T. Dinkova-Kostova, T. Efferth, K. El Bairi, N. Arkells, T.-P. Fan, B.L. Fiebich, M.
162 Freissmuth, M.I. Georgiev, S. Gibbons, K.M. Godfrey, C.W. Gruber, J. Heer, L.A. Huber,
163 E. Ibanez, A. Kijjoa, A.K. Kiss, A. Lu, F.A. Macias, M.J.S. Miller, A. Mocan, R. Müller,
164 F. Nicoletti, G. Perry, V. Pittalà, L. Rastrelli, M. Ristow, G.L. Russo, A.S. Silva, D.
165 Schuster, H. Sheridan, K. Skalicka-Woźniak, L. Skaltsounis, E. Sobarzo-Sánchez, D.S.
166 Bredt, H. Stuppner, A. Sureda, N.T. Tzvetkov, R.A. Vacca, B.B. Aggarwal, M. Battino,
167 F. Giampieri, M. Wink, J.-L. Wolfender, J. Xiao, A.W.K. Yeung, G. Lizard, M.A. Popp,
168 M. Heinrich, I. Berindan-Neagoe, M. Stadler, M. Daglia, R. Verpoorte, C.T. Supuran, T.
169 the International Natural Product Sciences, Natural products in drug discovery: advances
170 and opportunities, Nature Reviews Drug Discovery, 20 (2021) 200-216.
171 [47] B. Chopra, A.K. Dhingra, Natural products: A lead for drug discovery and
172 development, Phytother. Res., 35 (2021) 4660-4702.
173 [48] K. Dzobo, The Role of Natural Products as Sources of Therapeutic Agents for
174 Innovative Drug Discovery, Comprehensive Pharmacology, (2022) 408-422.
175 [49] A.R. Carroll, B.R. Copp, R.A. Davis, R.A. Keyzers, M.R. Prinsep, Marine natural
176 products, Natural Product Reports, (2022).
177 [50] W.-Y. Lu, H.-J. Li, Q.-Y. Li, Y.-C. Wu, Application of marine natural products in
178 drug research, Biorg. Med. Chem., 35 (2021) 116058.
179 [51] J.A. Nweze, F.N. Mbaoji, Y.-M. Li, L.-Y. Yang, S.-S. Huang, V.N. Chigor, E.A.
180 Eze, L.-X. Pan, T. Zhang, D.-F. Yang, Potentials of marine natural products against

malaria, leishmaniasis, and trypanosomiasis parasites: a review of recent articles, Infectious Diseases of Poverty, 10 (2021) 1-19.
[52] Y. Deng, Y. Liu, J. Li, X. Wang, S. He, X. Yan, Y. Shi, W. Zhang, L. Ding, Marine natural products and their synthetic analogs as promising antibiofilm agents for antibiotics discovery and development, European Journal of Medicinal Chemistry, (2022) 114513.
[53] M.A. Ghareeb, M.A. Tammam, A. El-Demerdash, A.G. Atanasov, Insights about clinically approved and Preclinically investigated marine natural products, Current Research in Biotechnology, 2 (2020) 88-102.
[54] N. Papon, B.R. Copp, V. Courdavault, Marine drugs: Biology, pipelines, current and future prospects for production, Biotechnol. Adv., 54 (2022) 107871.
[55] S. Begum, S. Hemalatha, Marine Natural Products—a Vital Source of Novel Biotherapeutics, Current Pharmacology Reports, (2022) 1-11.
[56] R.J. Andersen, D.J. Faulkner, C.H. He, G.D. Van Duyne, J. Clardy, Metabolites of the marine prosobranch mollusk Lamellaria sp, Journal of the American Chemical Society, 107 (1985) 5492-5495.
[57] C. Bailly, Curr. Med. Chem, Anti-cancer Agents, 4 (2004) 363-378.
[58] C. Bailly, Lamellarins, from A to Z: a family of anticancer marine pyrrole alkaloids, Current Medicinal Chemistry-Anti-Cancer Agents, 4 (2004) 363-378.
[59] P. Cironi, F. Albericio, M. Álvarez, Chapter 1 Lamellarins: Isolation, activity and synthesis, in: G. Gordon W, J. John A (Eds.) Prog. Heterocycl. Chem., Elsevier, 2005, pp. 1-26.
[60] T. Fukuda, F. Ishibashi, M. Iwao, Lamellarin alkaloids: Isolation, synthesis, and biological activity, The Alkaloids: Chemistry and Biology, 83 (2020) 1-112.
[61] C. Bailly, Lamellarins: A tribe of bioactive marine natural products, Outstanding Marine Molecules, (2014) 377-386.
[62] H. Fan, J. Peng, M.T. Hamann, J.-F. Hu, Lamellarins and related pyrrole-derived alkaloids from marine organisms, Chem. Rev., 108 (2008) 264-287.
[63] C. Tardy, M. Facompré, W. Laine, B. Baldeyrou, D. García-Gravalos, A. Francesch, C. Mateo, A. Pastor, J.A. Jiménez, I. Manzanares, Topoisomerase I-mediated DNA cleavage as a guide to the development of antitumor agents derived from the marine alkaloid lamellarin D: triester derivatives incorporating amino acid residues, Biorg. Med. Chem., 12 (2004) 1697-1712.

[64] J. Kluza, M.-A. Gallego, A. Loyens, J.-C. Beauvillain, J.-M.F. Sousa-Faro, C. Cuevas, P. Marchetti, C. Bailly, Cancer cell mitochondria are direct proapoptotic targets for the marine antitumor drug lamellarin D, Cancer Res., 66 (2006) 3177-3187.

[65] C. Imperatore, A. Aiello, F. D'Aniello, M. Senese, M. Menna, Alkaloids from marine invertebrates as important leads for anticancer drugs discovery and development, Molecules, 19 (2014) 20391-20423.

[66] C. Bailly, Anticancer properties of lamellarins, Mar. Drugs, 13 (2015) 1105-1123.

[67] S. Khiati, Y. Seol, K. Agama, I. Dalla Rosa, S. Agrawal, K. Fesen, H. Zhang, K.C. Neuman, Y. Pommier, Poisoning of mitochondrial topoisomerase I by lamellarin D, Mol. Pharmacol., 86 (2014) 193-199.

[68] M. Bayet-Robert, S. Lim, C. Barthomeuf, D. Morvan, Biochemical disorders induced by cytotoxic marine natural products in breast cancer cells as revealed by proton NMR spectroscopy-based metabolomics, Biochem. Pharmacol., 80 (2010) 1170-1179.

[69] C. Ballot, J. Kluza, S. Lancel, A. Martoriati, S.M. Hassoun, L. Mortier, J.-C. Vienne, G. Briand, P. Formstecher, C. Bailly, R. Nevière, P. Marchetti, Inhibition of mitochondrial respiration mediates apoptosis induced by the anti-tumoral alkaloid lamellarin D, Apoptosis, 15 (2010) 769-781.

[70] K. Yoshida, R. Itoyama, M. Yamahira, J. Tanaka, N. Loaëc, O. Lozach, E. Durieu, T. Fukuda, F. Ishibashi, L. Meijer, M. Iwao, Synthesis, Resolution, and Biological Evaluation of Atropisomeric (aR)- and (aS)-16-Methyllamellarins N: Unique Effects of the Axial Chirality on the Selectivity of Protein Kinases Inhibition, J. Med. Chem., 56 (2013) 7289-7301.

[71] D. Baunbæk, N. Trinkler, Y. Ferandin, O. Lozach, P. Ploypradith, S. Rucirawat, F. Ishibashi, M. Iwao, L. Meijer, Anticancer Alkaloid Lamellarins Inhibit Protein Kinases, Mar. Drugs, 6 (2008) 514-527.

[72] C. Neagoie, E. Vedrenne, F. Buron, J.-Y. Mérour, S. Rosca, S. Bourg, O. Lozach, L. Meijer, B. Baldeyrou, A. Lansiaux, S. Routier, Synthesis of chromeno[3,4-b]indoles as Lamellarin D analogues : A novel DYRK1A inhibitor class, European Journal of Medicinal Chemistry, 49 (2012) 379-396.

[73] H. Zhang, M.M. Conte, X.-C. Huang, Z. Khalil, R.J. Capon, A search for BACE inhibitors reveals new biosynthetically related pyrrolidones, furanones and pyrroles from a southern Australian marine sponge, Ianthella sp, Organic & Biomolecular Chemistry, 10 (2012) 2656-2663.

[74] A.R. Quesada, M.D. García Grávalos, J.L. Fernández Puentes, Polyaromatic alkaloids from marine invertebrates as cytotoxic compounds and inhibitors of multidrug resistance caused by P-glycoprotein, Br. J. Cancer, 74 (1996) 677-682.
[75] X.-C. Huang, X. Xiao, Y.-K. Zhang, T.T. Talele, A.A. Salim, Z.-S. Chen, R.J. Capon, Lamellarin O, a Pyrrole Alkaloid from an Australian Marine Sponge, Ianthella sp., Reverses BCRP Mediated Drug Resistance in Cancer Cells, Mar. Drugs, 12 (2014) 3818-3837.
[76] M.V.R. Reddy, M.R. Rao, D. Rhodes, M.S. Hansen, K. Rubins, F.D. Bushman, Y. Venkateswarlu, D.J. Faulkner, Lamellarin α 20-sulfate, an inhibitor of HIV-1 integrase active against HIV-1 virus in cell culture, J. Med. Chem., 42 (1999) 1901-1907.
[77] C.P. Ridley, M.V.R. Reddy, G. Rocha, F.D. Bushman, D.J. Faulkner, Total synthesis and evaluation of lamellarin α 20-Sulfate analogues, Biorg. Med. Chem., 10 (2002) 3285-3290.
[78] H. Kamiyama, Y. Kubo, H. Sato, N. Yamamoto, T. Fukuda, F. Ishibashi, M. Iwao, Synthesis, structure–activity relationships, and mechanism of action of anti-HIV-1 lamellarin α 20-sulfate analogues, Biorg. Med. Chem., 19 (2011) 7541-7550.
[79] C. Eurtivong, K. Choowongkomon, P. Ploypradith, S. Ruchirawat, Molecular docking study of lamellarin analogues and identification of potential inhibitors of HIV-1 integrase strand transfer complex by virtual screening, Heliyon, 5 (2019) e02811.
[80] A. El-Demerdash, S. Petek, C. Debitus, A. Al-Mourabit, Fatty Acids Pattern from the French Polynesian Monanchora n. sp. Marine Sponge, Chem. Nat. Compd., 54 (2018) 1143-1145.
[81] A. El-Demerdash, S. Petek, C. Debitus, A. Al-Mourabit, Crambescidin Acid from the French Polynesian Monanchora n. sp. Marine Sponge, Chem. Nat. Compd., 56 (2020) 1180-1182.
[82] A. El-Demerdash, L. Ermolenko, E. Gros, P. Retailleau, B.N. Thanh, G.-B. Anne, A. Al-Mourabit, Short-Cut Bio-Inspired Synthesis of Tricyclic Guanidinic Motifs of Crambescidins and Batzelladines Marine Alkaloids, Eur. J. Org. Chem., n/a.
[83] A.W.K. Yeung, A. El-Demerdash, I. Berindan-Neagoe, A.G. Atanasov, Y.-S. Ho, Molecular responses of cancers by natural products: modifications of autophagy revealed by literature analysis, Critical Reviews™ in Oncogenesis, 23 (2018).
[84] M. Sebak, F. Molham, M.A. Tammam, A. El-Demerdash, Chemical Diversity and Biological Activities of Anthraquinones Derived from Marine Fungi: A Comprehensive Update, (2022).

[85] A. El-Demerdash, C. Moriou, J. Toullec, M. Besson, S. Soulet, N. Schmitt, S. Petek, D. Lecchini, C. Debitus, A. Al-Mourabit, Bioactive Bromotyrosine-Derived Alkaloids from the Polynesian Sponge Suberea ianthelliformis, Mar. Drugs, 16 (2018) 146.
[86] A. El-Demerdash, A.M. Metwaly, A. Hassan, T.M. Abd El-Aziz, E.B. Elkaeed, I.H. Eissa, R.K. Arafa, J.D. Stockand, Comprehensive Virtual Screening of the Antiviral Potentialities of Marine Polycyclic Guanidine Alkaloids against SARS-CoV-2 (COVID-19), Biomolecules, 11 (2021) 460.
[87] A. El-Demerdash, A. Hassan, T.M. Abd El-Aziz, J.D. Stockand, R.K. Arafa, Marine Brominated Tyrosine Alkaloids as Promising Inhibitors of SARS-CoV-2, Molecules, 26 (2021) 6171.
[88] A. El-Demerdash, A.A. Al-Karmalawy, T.M. Abdel-Aziz, S.S. Elhady, K.M. Darwish, A.H. Hassan, Investigating the structure–activity relationship of marine natural polyketides as promising SARS-CoV-2 main protease inhibitors, RSC Advances, 11 (2021) 31339-31363.
[89] A.M. Elgohary, A.A. Elfiky, F. Pereira, T.M. Abd El-Aziz, M. Sobeh, R.K. Arafa, A. El-Demerdash, Investigating the structure-activity relationship of marine polycyclic batzelladine alkaloids as promising inhibitors for SARS-CoV-2 main protease (Mpro), Comput. Biol. Med., (2022) 105738.
[90] M. Frisch, G. Trucks, H. Schlegel, Gaussian 09, Revision B. 01 and Revision D. 01, Wallingford CT: Gaussian, (2010).
[91] A.D. Becke, A new mixing of Hartree–Fock and local density-functional theories, The Journal of chemical physics, 98 (1993) 1372-1377.
[92] A. Becke, Density-functional thermochemistry. III The role of exact exchange J Chem Phys 98: 5648–5652, in, 1993.
[93] N.M. O'Boyle, M. Banck, C.A. James, C. Morley, T. Vandermeersch, G.R. Hutchison, Open Babel: An open chemical toolbox, Journal of cheminformatics, 3 (2011) 1-14.
[94] O. Trott, A.J. Olson, AutoDock Vina: improving the speed and accuracy of docking with a new scoring function, efficient optimization, and multithreading, J. Comput. Chem., 31 (2010) 455-461.
[95] E.F. Pettersen, T.D. Goddard, C.C. Huang, G.S. Couch, D.M. Greenblatt, E.C. Meng, T.E. Ferrin, UCSF Chimera—a visualization system for exploratory research and analysis, J. Comput. Chem., 25 (2004) 1605-1612.

[96] A.C. Wallace, R.A. Laskowski, J.M. Thornton, LIGPLOT: a program to generate schematic diagrams of protein-ligand interactions, Protein engineering, design and selection, 8 (1995) 127-134.
[97] L. Abraham, B. Hess, V. Spoel, GROMACS 2020.3 source code. Zenodo, in, 2020.
[98] B. Miller, T. McGee, J. Swails, N. Homeyer, H. Gohlke i A. Roitberg, J Chem Theory Comput, 8 (2012) 3314-3321.
[99] M.S. Valdés-Tresanco, M.E. Valdés-Tresanco, P.A. Valiente, E. Moreno, gmx_MMPBSA: a new tool to perform end-state free energy calculations with GROMACS, Journal of chemical theory and computation, 17 (2021) 6281-6291.
[100] A. Daina, O. Michielin, V. Zoete, SwissADME: a free web tool to evaluate pharmacokinetics, drug-likeness and medicinal chemistry friendliness of small molecules, Scientific reports, 7 (2017) 1-13.
[101] F. Ishibashi, S. Tanabe, T. Oda, M. Iwao, Synthesis and structure-activity relationship study of lamellarin derivatives, Journal of Natural Products, 65 (2002) 500-504.
[102] C.P. Ridley, M.V.R. Reddy, G. Rocha, F.D. Bushman, D.J. Faulkner, Total synthesis and evaluation of lamellarin alpha 20-sulfate analogues, Bioorganic & Medicinal Chemistry, 10 (2002) 3285-3290.
[103] C. Bailly, Lamellarins, from A to Z: a family of anticancer marine pyrrole alkaloids, Current medicinal chemistry. Anti-cancer agents, 4 (2004) 363-378.
[104] W. Humphrey, A. Dalke, K. Schulten, VMD: visual molecular dynamics, J. Mol. Graphics, 14 (1996) 33-38.
[105] T. Fukuda, F. Ishibashi, M. Iwao, Lamellarin alkaloids: Isolation, synthesis, and biological activity, The Alkaloids. Chemistry and biology, 83 (2020) 1-112.
[106] I. Satyanarayana, D.-Y. Yang, T.-J. Liou, Synthesis of lamellarin R, lukianol A, lamellarin O and their analogues, RSC advances, 10 (2020) 43168-43174.
[107] J.R. Hwu, A. Roy, A. Panja, W.-C. Huang, Y.-C. Hu, K.-T. Tan, C.-C. Lin, K.-C. Hwang, M.-H. Hsu, S.-C. Tsay, Domino Reaction for the Synthesis of Polysubstituted Pyrroles and Lamellarin R, The Journal of Organic Chemistry, 85 (2020) 9835-9843.
[108] Z. Liu, X. Liu, S. Yang, X. Miao, D. Li, D. Wang, Titanium-Mediated aza-Nazarov Annulation for the Synthesis of N-Fused Tricycles: A General Method to Access Lamellarin Analogues, The Journal of Organic Chemistry, (2022).

346 [109] J.W. Jhang, K.B. Manjappa, D.Y. Yang, Synthesis of Naphthoquinone-and Pyrrolo
347 [2, 1-a] isoquinoline-Fused Heterocycles and Tridemethoxy Lamellarin D, Asian Journal
348 of Organic Chemistry, 11 (2022) e202100660.

349